




Collision efficiency of cloud droplets in quiescent air considering lubrication interactions, mobility of interfaces, and noncontinuum molecular effects

Ahmad Ababaei ^{*} and Bogdan Rosa [†]*Institute of Meteorology and Water Management – National Research Institute,
Podleśna 61, 01-673 Warsaw, Poland* (Received 19 August 2022; accepted 22 December 2022; published 17 January 2023)

The collision efficiency of cloud droplets settling under gravity in quiescent air is investigated by means of numerical simulations. In the developed model, the droplets are represented as either rigid spheres or nondeformable liquid particles of finite viscosity. For the latter, both the internal circulation of the fluid and the mobility of interfaces are accounted for. The aerodynamic interaction, resulting from relative motion of the particles in a viscous medium, is evaluated by making use of a Stokes flow solution. The effect of noncontinuum lubrication for the flow in the gap between surfaces of the droplets is also analyzed. This provides a more physical description of aerodynamic interactions valid for a wide range of the Knudsen number and gap sizes. In contrast to an earlier study by Rother *et al.* [*Int. J. Multiphase Flow* **146**, 103876 (2022)], noncontinuum lubrication and internal circulation effects have been analyzed separately. Additionally, rotational motion is considered for rigid particles. An objective comparison of the obtained results with the reference data has been performed as well. Compared to the standard continuum description of aerodynamic interaction for nonrotating rigid spherical particles, noncontinuum lubrication and internal circulation effects both lead to a larger collision efficiency, whereas rotation reduces collision efficiency. In general, noncontinuum lubrication has a larger impact on the collision efficiency compared to the internal circulation of drops, which loses its influence as their inertia (size) increases. In numerical simulations, therefore, treating medium-sized cloud droplets as rigid particles is an accurate assumption, but considering noncontinuum effects in their aerodynamic interaction is expected to alter the results. In the limit of a large viscosity ratio, the values of collision efficiency for the liquid drops and freely rotating rigid particles are in a quantitative agreement. Numerical aspects are also discussed, with a focus on assessing computational complexity and algorithm parallelization. The simplified problem studied here is an important step towards improving the representation of aerodynamic interaction in systems with a large number of droplets interacting in a turbulent flow.

DOI: [10.1103/PhysRevFluids.8.014102](https://doi.org/10.1103/PhysRevFluids.8.014102)

I. INTRODUCTION

Thermodynamic processes in the atmosphere constitute the weather and climate of a given area. These processes are influenced by many factors such as orography, the vicinity of water bodies, or the presence of various types of clouds. Clouds govern precipitations, contribute to the water cycle, and influence the Earth's radiative properties, to name but a few examples [1].

* ahmad.ababaei@imgw.pl

[†]Also at the Department of Applied Mathematics, Warsaw University of Life Sciences, 02-776 Warsaw, Poland

The role of clouds in the atmospheric processes extends over a wide range of temporal and spatial scales. The quantitative description of such multiscale phenomena is a challenging task requiring a special experimental facility and advanced modeling techniques [2]. Knowledge in this area, in turn, is essential for the development of reliable weather and climate forecasts. Of particular interest are the microphysical effects related to both droplet-droplet and droplet-air interactions. The small-scale processes determine the collision rate and consequently the precipitation formation [3]. These phenomena cannot be resolved in the numerical weather prediction (NWP) systems since the horizontal grid spacing of these models is of the order of one kilometer.

In recent decades, considerable research has been conducted to quantify the cloud microphysical processes under different atmospheric conditions [4–6]. Their accurate description is important to develop a more realistic parametrization for the NWP models. Despite enormous efforts and advancements in research methods, knowledge in the area remains insufficient. Of specific attention are the mechanisms that lead to a fast broadening of droplet size distribution, including the entrainment mixing of unsaturated air with the cloud [7], the effects of giant aerosol particles [8], turbulent fluctuations of the water-vapor supersaturation [9], and turbulent collision-coalescence [10]. Growth of the medium-sized droplets, 10–60 μm in radii, is driven mainly by turbulent collisions. The turbulent flow enhances the radial relative velocity and alters spatial distribution of the droplets [11]. Under certain conditions, the disturbance generated by the moving particles also has an important effect on the collision efficiency [12]. Yet an important factor often neglected in numerical models is the aerodynamic interaction.

The aim of this study is to investigate the effects of aerodynamic interaction, noncontinuum lubrication (NCL), and internal circulation of fluid droplets (FDs) on the collision efficiency of a pair of inertial water droplets settling under gravity in quiescent air. Doing so leads to an in-depth understanding of how an improved representation of aerodynamic interaction affects collision. This is an intermediate step enabling us to extend the problem to a more general case of a large number of droplets interacting in a turbulent field of air.

In the most common numerical approach, the dynamics of cloud droplets is governed by the Stokes equation. This approximation is sufficient in the limit of low Reynolds number where inertial effects can be safely neglected [13]. Due to high complexity of particle-particle and particle-fluid interactions at a wide range of spatiotemporal scales, the analytical solution to the Stokes equation can be easily derived only for a single particle in a uniform flow. To represent the dynamics of systems with many mutually interacting particles several approximate approaches have been proposed. The most common one is the *superposition method* [14], in which the net drag force acting on a given particle is evaluated by considering perturbations generated by all other particles in its proximity. The superposition method was improved by Wang *et al.* [15] and then found application in the so-called hybrid direct numerical simulations introduced by Ayala *et al.* [16]. While accurate for droplets interacting from large separation distances, superposition methods do not precisely predict the drag forces when they are very close to each other. This inaccuracy stems from the superposition of the Stokes solutions that represent the flow around a *single* isolated sphere. In the literature, there are several studies that provide exact solutions to the Stokes equation for *two* interacting particles. A brief review of the prominent exact solutions to the two-sphere problems is deferred until Appendix A.

The studies that have particularly focused on two spheres approaching (or retreating) along their line of centers, e.g., Maude [17], predict resistance coefficients that grow without bound as the gap between the pair diminishes. This singular behavior prevents the collision under a constant force applied within finite time [18,19]. To avoid this problem in the numerical models additional treatments are needed. One of the remedies is to cut these singular resistances at a specific gap size, thereby ignoring any further increase in the lubrication force beyond this limit. For instance, the *collision gap model* assumes that the collision takes place when the gap between the pair is smaller than a tiny predefined value [20]. Another approach to overcome the lubrication singularity is to include the attractive van der Waals forces [13,21]. Rosa *et al.* [21] showed that the collision gap

model leads to an underestimation in the collision efficiency compared to the simulations with van der Waals forces.

The vast majority of solutions to the Stokes equation that predict lubrication forces are based on the assumption that the fluid is a continuous medium. However, when the gap between the droplets is comparable to the mean-free path of the fluid's molecules, the continuum mechanical theories are no longer valid [19,22], and the exact analytical solutions lose their accuracy. At such gaps the discrete molecular character of the fluid, i.e., noncontinuum effects, must be considered. This results in lubrication resistance increasing with the inverse of the gap size at a much slower logarithmic pace [13], leading to lower forces compared with the drag from continuum-based solutions. Therefore, once noncontinuum effects are considered, the particles are able to make contact within finite time [19,23,24]. Sundararajakumar and Koch [19] solved the flows under different noncontinuum regimes depending on the size of the gap, providing analytical expressions for pressure distribution and drag force. Dhanasekaran *et al.* [23] fitted a function to these solutions in such a way that it uniformly covers all the regimes by smooth transitions. These solutions are valid for large Knudsen numbers.

The lubrication forces are also modified when the internal circulation of droplets is taken into consideration. Instead of an increase inversely proportional to the gap size derived for rigid spheres, it has been shown that the growth in lubrication forces acting on a pair of spherical fluid drops is inversely proportional to the square root of the separation distance [18,25]. Accordingly, collision is possible within finite time under an exerted constant force. Haber *et al.* [26] developed the exact solution to two unequal fluid drops having different viscosities and moving with any orientation along their line of centers. An exact solution to the translation of such a pair normal to their line of centers was derived by Zinchenko [27]. Taken together these two studies yield an exact representation for the forces acting on two fluid drops interacting inside a viscous flow. Using these solutions, Zinchenko [28] assessed the collision efficiency for a noninertial pair of droplets. In a recent study, Rother *et al.* [6] computed the collision efficiency of an inertial pair of fluid droplets taking into account Maxwell slip and van der Waals forces. Thus, in their approach both effects, internal circulation and noncontinuum lubrication, albeit limited to low Kn , were considered simultaneously. The aim of the present study is to examine each effect separately and assess their significance on the collision efficiency. Additionally, we address the impact of particle rotation at different ranges of the radii ratio and inertia. The results will be compared with the reference data of Rother *et al.* [6] and those calculated using the approximate model developed by Wang *et al.* [15], which is accurate for widely spaced particles (droplets).

The remainder of the article is organized as follows. Section II describes the methodology to compute the collision efficiency, the equations of motion, and force representations used in the simulations. The first part of Sec. III focuses on a detailed comparison between various representations for aerodynamic interaction. Then the results of simulations are presented and discussed. The second part of Sec. III deals with numerical aspects of simulations, including computation time and improvements to the algorithm. Finally, Sec. IV states the key conclusions drawn from this study.

II. METHODOLOGY

The numerical method for computing the collision efficiency is based on Lagrangian particle tracking. In the modeled system, the relative motion of two unequal aerodynamically interacting droplets settling under gravity in quiescent air is considered. The droplets are treated as nondeformably spherical particles that are either fluid (having an internal Stokesian circulation) or rigid (nondeformable and solid). The larger droplet assumed here is of radii $a_1 = 10, 20,$ and $30 \mu\text{m}$, while the radii of the smaller one are defined by the parameter $\lambda = a_2/a_1$. In each simulation series, λ varies in the range $0.05 \leq \lambda \leq 0.99$. For such a setting the inertia of the surrounding fluid, i.e., air, is negligible. To compute the collision efficiency, the far-field off-center horizontal separations for the grazing trajectories need to be determined. In other words, it is necessary to find the maximum horizontal shift beyond the area of aerodynamic interaction for which the collision of the droplets

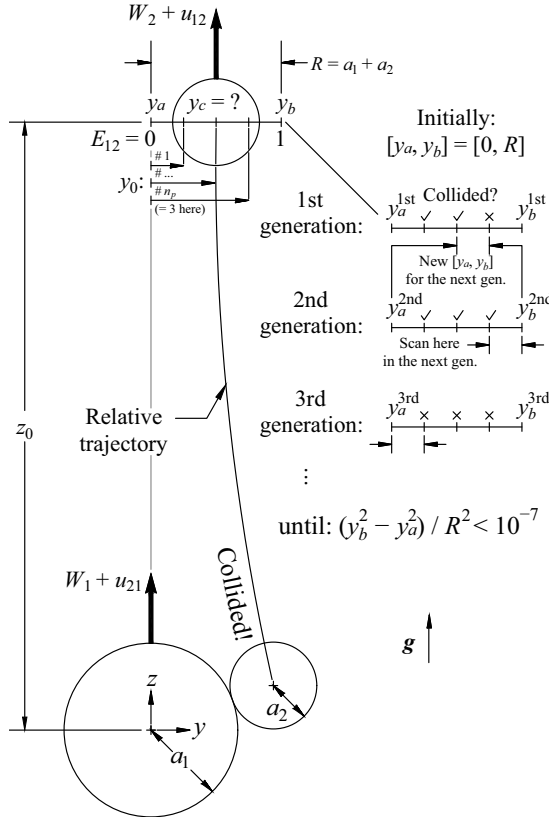


FIG. 1. A parallel procedure, with $n_p = 3$, for evaluation of collision efficiency

may occur. To find this, a modified bisection method was employed. The simulations were initialized with arbitrary values of the shift and successively corrected based on the information whether the droplets collided or not. Each iteration in this procedure is called a generation. Since the collision efficiency is very sensitive to small differences in aerodynamic interaction representations, it is expected that the noncontinuum effects or the internal circulation of water inside droplets will have a noticeable impact on the probability of collision. Thus, these effects will be examined by employing force representation models derived based on each effect. Still, the physical properties of surrounding air and water droplets, including the densities $\rho_f = 1.3 \times 10^{-3}$ and $\rho_i = 1 \text{ g/cm}^3$, and the dynamic viscosity $\mu_f = 1.7 \times 10^{-4} \text{ g/(cm s)}$, remain the same in all simulations. Moreover, two values, $\mu_i = 100\mu_f$ and $\mu_i \rightarrow \infty$, are assumed for the dynamic viscosity of water when the internal circulation of droplets is taken into consideration. This model offers a basic understanding of the interaction between a pair of droplets, which can be later employed in a many-body system of interacting droplets.

A. Numerical method

Figure 1 illustrates the methodology to evaluate the collision efficiency. A parallel scanning procedure is used to speed up the convergence rate. Initially, the larger droplet is placed at the origin, $\mathbf{Y}_1 = (0, 0, 0)$ and several smaller ones at $\mathbf{Y}_2 = (0, y_0, z_0)$, each setting being an independent problem. The initial vertical separation is always the same and equal to $z_0 = 50R$, where $R = a_1 + a_2$. This distance is large enough to ensure that the collision efficiency does not depend on the initial vertical separation distance. As for the initial horizontal separation distance $y_0(t = 0)$, different

values are simultaneously considered, $y_0^{(1)}, \dots, y_0^{(n_p)}$. This configuration comes down to placing n_p smaller droplets at equally spaced distances within the entire possible (initial) range of collision, namely, $[0, R]$. Here n_p is the number of processes (subgenerations) per each generation. The initial velocities are the terminal velocity of each droplet to which the Stokes disturbance of the other droplet is added to ensure that collision efficiency and droplet trajectories are independent from the initial vertical separation distance, z_0 . These settings reduce the three-dimensional problem to a quasi-two-dimensional one with the droplets moving only in a y - z plane and rotating around the axis pointed in the x direction. Every subgeneration independently begins to evolve by integrating the equations of motion for each pair of droplets. An entire generation finishes once all of its subgenerations are completed with an outcome, either a collision or not. Based on this information, the range of y_0 is narrowed down for the next generation. This procedure continues until the range is narrow enough, where the maximum initial horizontal separation distance leading to a collision, $y_c (\approx y_b \approx y_a)$, is found, providing an estimation for collision efficiency [14]:

$$E_{12} = \frac{y_c^2}{R^2}.$$

The collision efficiency can alternatively be defined based on the size of larger droplet as $E'_{12} = y_c^2/a_1^2 = E_{12}(1 + \lambda)^2$, which can be greater than unity [29].

B. Equations of motion

The acceleration of a pair of inertial particles can be expressed using the following compact notation:

$$\frac{d\mathbf{V}_i}{dt} = \left(1 - \frac{\rho_f}{\rho_i}\right)\mathbf{g} + \frac{\mathbf{F}_i}{m_i}, \quad (i = 1, 2), \quad (1)$$

where the first term on the r.h.s. includes gravity and buoyancy. The second term handles all the other forces e.g., attractive van der Waals forces, hydrodynamic (aerodynamic, in this case) interaction between the particles (water droplets), etc.

Treating a rigid sphere as a special case, the drag force (F_i^s , where s stands for single sphere) exerted by a fluid of viscosity μ_f on an isolated spherical fluid drop of viscosity μ_i is (Hadamard–Rybczyński problem in Sec. 4.9 of Ref. [30] or Example 4.3 of Ref. [31])

$$F_i^s = -4\pi\mu_f a_i V_i \underbrace{\frac{\frac{3}{2}\hat{\mu}_r + 1}{\hat{\mu}_r + 1}}_{\hat{\mu}_d} = -4\pi\mu_{fd} a_i V_i, \quad (2)$$

where $\hat{\mu}_r \equiv \frac{\mu_i}{\mu_f}$ is the viscosity ratio and $\mu_{fd} \equiv \mu_f \hat{\mu}_d$ is a factor defined for convenience to avoid repetition. Here “hats” indicate the values that are dimensionless. The special case of Stokes drag acting on a rigid sphere, $-6\pi\mu_f a_i V_i$, is recovered when $\hat{\mu}_r \rightarrow \infty$ [31]. Based on Eq. (2), the fluid droplet inertial response time is defined as

$$\tau_i \equiv \frac{m_i}{4\pi\mu_{fd} a_i}, \quad (3)$$

yielding terminal velocities

$$W_i = \left(1 - \frac{\rho_f}{\rho_i}\right)\tau_i g. \quad (4)$$

It is worth noting that the inertia (τ_i) of the liquid particle (fluid drop) is larger than that of the rigid particle, and thus its settling velocity is correspondingly faster.

Equation (1) can be rewritten using the definitions given in (3) and (4). Moreover, the force representing the aerodynamic interaction (F_i^{AI}) can be normalized by the Stokes drag factor for a

single spherical fluid drop and then expressed in terms of the velocity perturbation, namely, $u_i \equiv F_i^{AI} / -4\pi\mu_f a_i$. Accordingly, the equations of motion for a pair of particles reduce to

$$\frac{d\mathbf{V}_i}{dt} = \frac{\mathbf{W}_i - \mathbf{u}_i}{\tau_i}, \quad (5)$$

$$\frac{d\mathbf{Y}_i}{dt} = \mathbf{V}_i, \quad (6)$$

$$\frac{d\boldsymbol{\Omega}_i}{dt} = \frac{\mathbf{T}_i}{I_i} \quad (\text{only rigid}). \quad (7)$$

Here \mathbf{Y}_i and \mathbf{V}_i denote the position and velocity of the droplets, respectively. Equation (7) applies only to rigid spherical particles with angular velocities, torques, and moments of inertia referred to by $\boldsymbol{\Omega}_i$, \mathbf{T}_i , and I_i , correspondingly. For fluid drops, this equation must be replaced with $d\mathbf{L}/dt = \mathbf{T}$ where the angular momentum is defined as $\mathbf{L} = \int_V \mathbf{r} \times \mathbf{U} \rho dV$ over the drop volume, with \mathbf{r} being the radial vector from the center of the drop and \mathbf{U} the surrounding fluid velocity. Zinchenko [27] proved that the hydrodynamic torque acting on a fluid drop is always zero. The proof holds even for a Navier-Stokes flow inside each drop:

$$\mathbf{T} = \oint_S \mathbf{r} \times \boldsymbol{\sigma}_f^{(\hat{n})} dS, \quad (8a)$$

$$= \int_V \mathbf{r} \times \nabla \cdot \boldsymbol{\sigma}_i dV, \quad (8b)$$

$$= \int_V \mathbf{r} \times \rho \frac{D\mathbf{U}}{Dt} dV, \quad (8c)$$

$$= \frac{d\mathbf{L}}{dt}, \quad (8d)$$

which is zero in the case of Stokes flow, $\nabla \cdot \boldsymbol{\sigma}_i = 0$, where $\boldsymbol{\sigma}$ is the stress tensor and $\boldsymbol{\sigma}^{(\hat{n})}$ is the stress vector on the surface dS . Note that Eq. (8b) switches the integration over the external to the internal surface of the drop owing to tangential stress continuity and employs the Gauss theorem to transform this into a volume integral [27]. Since angular momentum is automatically conserved for a fluid drop, there is no need to solve an equation equivalent to Eq. (7) even for a massive drop with inertia. Moreover, the hydrodynamic torque vanishes when the internal circulation is approximated as a Stokes flow. This is plausible for small atmospheric drops due only to their large dynamic viscosity ratio.

C. Force and torque representations

The terms representing the aerodynamic interaction in Eqs. (5)–(7) are evaluated using both approximate and exact solutions of the Stokes equation. The torque does not need to be evaluated if the droplet rotation is neglected. An approximate representation of the aerodynamic force is obtained using (1) the improved superposition method (ISM) of Wang *et al.* [15]. This method was originally developed for modeling systems comprising solid spherical particles. To employ the ISM for modeling the collision efficiency of water droplets, it first had to be generalized to the case of liquid particles. This method is based on the exact solution to the Stokes flow induced by a single translating sphere. Exact force representations utilized here are based on analytical solutions to the two-sphere problem. We used two alternative solutions available in the literature, namely, (2) the twin multipole expansion method and (3) solutions in bispherical coordinates system. Finally, we use (4) an accurate representation of AI which additionally accounts for the noncontinuum lubrication effects.

1. Hadamard-Rybczyński problem: Approximate representation

A Stokes disturbance field generated by a single nondeformably spherical fluid drop of radius a and dynamic viscosity μ_i moving at the velocity \mathbf{V} in a fluid of viscosity μ_f is [32,33]

$$\mathbf{u}_{\text{St}}(\mathbf{r}; a, \mathbf{V}) = \left[A_1 \left(\frac{a}{r} \right) - 3B_1 \left(\frac{a}{r} \right)^3 \right] \frac{\mathbf{V} \cdot \mathbf{r}}{r^2} \mathbf{r} + \left[A_1 \left(\frac{a}{r} \right) + B_1 \left(\frac{a}{r} \right)^3 \right] \mathbf{V}, \quad (9)$$

in which $r = \|\mathbf{r}\|$ is the magnitude of the vector connecting the center of the sphere to any arbitrary point at which the disturbance \mathbf{u}_{St} is felt; $A_1 = \frac{2+3\hat{\mu}_r}{4(1+\hat{\mu}_r)}$ and $B_1 = \frac{\hat{\mu}_r}{4(1+\hat{\mu}_r)}$ are derived in hydrodynamics textbooks (e.g., Example 4.3 in Kim and Karrila [31]). We note that in the limit $\hat{\mu}_r \rightarrow \infty$, Eq. (9) converges to the formula representing the Stokes disturbance field generated by a rigid sphere translating in a viscous fluid (Exercise 2.7 in Ref. [31]).

The ISM of Wang *et al.* [15] is generalized for spherical fluid drops by replacing the Stokes disturbance velocity field generated by a rigid sphere with Eq. (9). This yields an approximate representation for the forces acting on a pair of liquid, as well as solid, spheres. Since the ISM is based on the superposition of solutions for single spheres, the forces of aerodynamic interactions are accurate only for large separation distances. Nevertheless, the important advantage of ISM is its ability to be extended for a many-body system of interacting particles [16]. It should also be added that the rotational motion is intrinsically not handled by the ISM.

2. Resistance problem: Exact representation

The general resistance problem relates the forces and the torques acting on two spheres ($\mathbf{F}_i, \mathbf{T}_i$) to their linear and angular velocities ($\mathbf{V}_i, \boldsymbol{\Omega}_i$). This relation is given, for example by Jeffrey and Onishi [34] [Eq. (1.3) therein], as follows:

$$\begin{pmatrix} \mathbf{F}_1 \\ \mathbf{F}_2 \\ \mathbf{T}_1 \\ \mathbf{T}_2 \end{pmatrix} = \mu_f \begin{bmatrix} A_{11} & A_{12} & \tilde{\mathbf{B}}_{11} & \tilde{\mathbf{B}}_{12} \\ A_{21} & A_{22} & \tilde{\mathbf{B}}_{21} & \tilde{\mathbf{B}}_{22} \\ \mathbf{B}_{11} & \mathbf{B}_{12} & \mathbf{C}_{11} & \mathbf{C}_{12} \\ \mathbf{B}_{21} & \mathbf{B}_{22} & \mathbf{C}_{21} & \mathbf{C}_{22} \end{bmatrix} \begin{pmatrix} \mathbf{V}_1 \\ \mathbf{V}_2 \\ \boldsymbol{\Omega}_1 \\ \boldsymbol{\Omega}_2 \end{pmatrix}, \quad (10)$$

in which μ_f is the dynamic viscosity of the ambient fluid. The resistance tensors $A_{\alpha\beta}$, $\tilde{\mathbf{B}}_{\alpha\beta}$, $\mathbf{B}_{\alpha\beta}$, and $\mathbf{C}_{\alpha\beta}$ comprise the resistance functions $X_{\alpha\beta}^A$, $Y_{\alpha\beta}^A$, $Y_{\alpha\beta}^B$, $X_{\alpha\beta}^C$, and $Y_{\alpha\beta}^C$. A complete set of these functions for two rigid spheres assuming the no-slip boundary condition has been derived making use of twin multipole expansions [34]. Each function takes the form of a high-order series in inverse powers of center-to-center separation. The singularities are removed using asymptotic expressions that are valid for nearly touching spheres. The functions depend on the spheres radii ratio $\lambda = a_2/a_1$ and normalized separation distance $s = r/\frac{1}{2}(a_1 + a_2)$. Here r is the distance between the centers of the particles. The functions X and Y handle motion along the line of centers and normal to that, respectively. The indices α and β are integers $\{1, 2\}$, introduced to distinguish particles in the pair. These resistance functions provide an exact force-torque representation exerted on a pair of rigid spheres that is valid only in the limit of continuum fluid mechanics. Further on, we will discuss the noncontinuum lubrication description that is based on these resistances with a modified $X_{\alpha\beta}^A$ function.

3. Bispherical solutions: Exact representation

The literature offers a number of solutions, both partial for selected cases and complete, to the Stokes equation for a system of two interacting spheres. A brief survey of the exact solutions developed in bispherical coordinates is carried out in Appendix A. A few of them are employed in this study to obtain the accurate representation of the aerodynamic interactions. For example, the translational motion along the line joining particle centers is handled by an implicit implementation of Stimson and Jeffrey [35]. In turn, forces and torques driving the relative motion in the direction normal to the line of centers are obtained from O'Neill and Majumdar [36]. The complexity of the

modeled system can be significantly reduced by mapping particle motion onto a (2D) vertical plane. Due to the geometrical setting, there is neither rotation nor torque around the line of centers.

For modeling the motion of a pair of spherical drops, we use the methodology developed by Haber *et al.* [26] and Zinchenko [27]. These solutions enable us to calculate the interactions of particles in the direction parallel and perpendicular to the line connecting their centers. It is worth mentioning that these representations [26,27] have already been used to compute the collision efficiency of noninertial liquid spheres [28]. In this paper, we use the same method for a more general case, i.e., inertial droplets of unequal size.

4. Noncontinuum lubrication

The analytical solutions to the Stokes equation for two rigid spheres discussed above were developed assuming that the surrounding fluid is a continuous medium. This assumption is valid as long as the gap between the surfaces of the spheres is significantly larger than the mean-free path of the fluid molecules. When the collisions of cloud droplets are considered, the discrete molecular structure of air becomes important, and this effect needs to be adequately taken into account. In particular, consequences of noncontinuum interactions are the most pronounced for the squeezing flow, i.e., a pair of particles approaching each other. For the other types of motion, e.g., shearing flow, these effects are less important or even negligible. This is because the tangential mobilities, even under continuum hydrodynamics, remain finite at contact [23]. In general, the noncontinuum lubrication forces are lower, although the reduction depends on the gap between the spheres.

Depending on the thickness of the gap relative to the mean-free path of air molecules, the flow between the spheres falls in different regimes. Sundararajakumar and Koch [19] combined several approaches and computed the pressure distribution in the gap between spheres within a wide range of gap sizes. Then, the noncontinuum lubrication forces were derived via integrating the pressure over particle surfaces. Dhanasekaran *et al.* [23] have fitted a smooth function f^{nc} to these solutions [19], uniformly covering separation distances under different regimes (see Sec. 4.1 therein). This noncontinuum representation converges to the continuum one at large separations. Moreover, it is given in a convenient form as a generalization of the solution for a continuum flow regime in a bispherical coordinate system. A similar approach is adopted here for representing noncontinuum lubrication through the resistance functions of Jeffrey and Onishi [34]. For two nearly touching spheres the resistance functions [(3.17) and (3.18) therein] are

$$X_{11}^A = g_1(\lambda)\xi^{-1} + g_2(\lambda)\ln(\xi^{-1}) + X_{11}^{\text{ns}}, \quad (11)$$

$$X_{12}^A = \frac{-2}{1+\lambda} [g_1(\lambda)\xi^{-1} + g_2(\lambda)\ln(\xi^{-1}) + X_{12}^{\text{ns}}], \quad (12)$$

in which $\xi = h/\frac{1}{2}(a_1 + a_2) = s - 2$ is the normalized gap between the surfaces of two spheres, and the size of the gap is $h = r - (a_1 + a_2)$. The functions $g_1(\lambda) = 2\lambda^2/(1 + \lambda)^3$ and $g_2(\lambda) = \lambda(1 + 7\lambda + \lambda^2)/5(1 + \lambda)^3$ depend only on radii ratio, and X_{11}^{ns} and X_{12}^{ns} stand for the nonsingular terms in the resistance functions remaining finite as $\xi \rightarrow 0$. Conversely, the first two terms are singular with the second term having a much slower logarithmic growth rate. Taking noncontinuum effects into account, analogous to (4.5) and (4.6) of Dhanasekaran *et al.* [23], the first singular term will be replaced with the fit expression as follows:

$$X_{11}^{\text{nc}} = X_{11}^A + g_1(\lambda) \left(\frac{f^{\text{nc}}}{Kn} - \frac{1}{\xi} \right), \quad (13)$$

$$X_{12}^{\text{nc}} = X_{12}^A + \frac{-2}{1+\lambda} g_1(\lambda) \left(\frac{f^{\text{nc}}}{Kn} - \frac{1}{\xi} \right), \quad (14)$$

where

$$Kn \equiv \frac{l_m}{\frac{1}{2}(a_1 + a_2)} \quad (15)$$

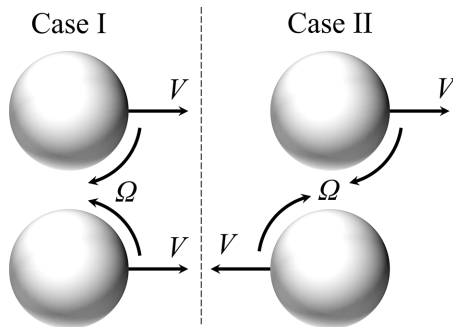


FIG. 2. Two symmetric cases of free rotation for a rigid pair.

is the Knudsen number representing the strength of noncontinuum effects, and l_m ($\approx 0.1 \mu\text{m}$ for air) is the mean-free path of molecules. The modified resistance functions, (13) and (14), yield the resistance for a rigid pair translating with an opposing orientation along their line of centers, $X_{11}^{\text{nc}} - \frac{1}{2}(1 + \lambda)X_{12}^{\text{nc}}$. However, they give a representation identical to the continuum one for a pair with the same orientation, $X_{11}^{\text{nc}} + \frac{1}{2}(1 + \lambda)X_{12}^{\text{nc}} = X_{11}^{\text{A}} + \frac{1}{2}(1 + \lambda)X_{12}^{\text{A}}$. In a range of low Knudsen numbers (Kn) of the order $O(10^{-1})$, Reed and Morrison [37] have obtained an analytical solution for this type of motion. Their solution is developed under a continuum assumption for the fluid with slip boundary condition at the surfaces of spheres. Since Kn for the smallest droplets considered in this study is about $O(10^{-2})$, this solution can be used to represent noncontinuum effects for a pair following each other along their line of centers.

D. Force acting on liquid particles in the limit of high-viscosity ratio

The drag force acting on a pair of spherical drops immersed in a viscous flow is a function of the viscosity ratio $\hat{\mu}_r$. When the viscosity of the fluid circulating inside the spheres greatly exceeds the viscosity of the external fluid, the dynamical properties (e.g., inertia) of these bodies become similar to those of rigid particles. In the limit of large $\hat{\mu}_r$, the drag forces predicted by the solution of Wacholder and Weihs [38] approach those resulting from the analytical solutions developed for rigid spheres (e.g., Stimson and Jeffery [35]). For a pair of particles interacting normal to their line of centers, the solution for liquid spheres (e.g., Zinchenko [27]) at high viscosity ratios corresponds to that of rigid particles (e.g., O'Neill and Majumdar [36]) only in a particular case that the rigid pair is undergoing *free rotation*. This was put forward by Zinchenko [27] based on the solution he developed for the normal interaction of a pair of liquid spheres. According to that study, the moments of hydrodynamic forces about the centers of mass of spheres are always zero, even in the limit of high $\hat{\mu}_r$. Therefore, the forces acting on liquid particles in the limit of high viscosity ratios must approach those due to translation of freely rotating rigid particles, because the net torque, i.e., sum of the torques caused by translation and rotation, acting on a pair of freely rotating rigid particles is zero.

A mathematical description of free rotation is presented here. Figure 2 shows two cases for an identical pair of rigid spheres symmetrically translating with velocity V perpendicular to their line of centers and rotating with Ω about their central axes that are normal to their line of centers. In both cases, if the torque due to translation is counterbalanced by an equal and opposite torque due to rotation, then the angular velocity Ω can be expressed in terms of translational velocity V as follows:

$$\frac{T}{-8\pi\mu a^2} = \hat{T}^{\text{tr}}V + \hat{T}^{\text{ro}}a\Omega = 0 \Rightarrow a\Omega = -\frac{\hat{T}^{\text{tr}}}{\hat{T}^{\text{ro}}}V. \quad (16)$$

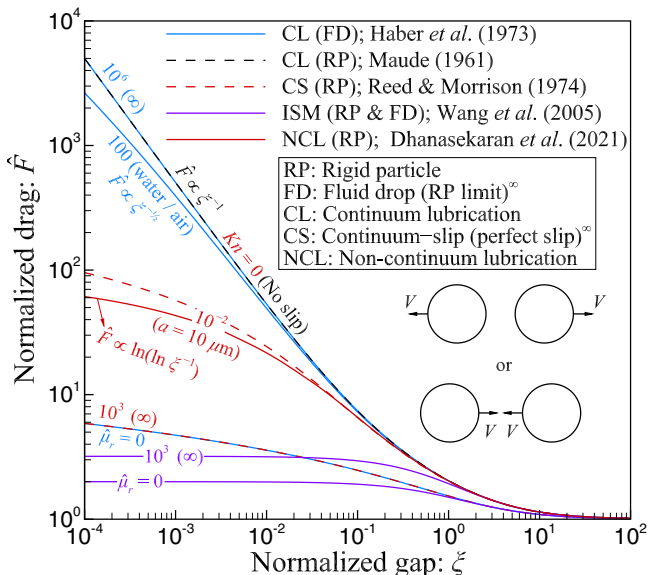


FIG. 3. Comparison of the normalized aerodynamic force (resistance) acting on a pair of equal-sized spherical drops moving with the same velocity but an opposing orientation along their line of centers. The approximate value (order) for the limit of each solution is marked with ∞ , indicating an insignificant change for a larger $\hat{\mu}_r$ or Kn .

Consequently, the net force due to translation and rotation would be

$$\frac{F}{-6\pi\mu a} = \hat{F}^{\text{tr}}V + \hat{F}^{\text{ro}}a\Omega = \left(\hat{F}^{\text{tr}} - \hat{F}^{\text{ro}} \frac{\hat{T}^{\text{tr}}}{\hat{T}^{\text{ro}}} \right) V, \quad (17)$$

which is smaller than $\hat{F}^{\text{tr}}V$, the force which would exist if the particles were merely translating, e.g., when rotation is neglected. Here \hat{F} and \hat{T} are nondimensional resistance coefficients for equal pairs [39,40]. Note that the translational and rotational orientations of the pair differ; namely, if the pair is translating with equal velocities in the same direction, the angular velocities are equal but have opposite signs, and vice versa. Such a simple description is possible only when the problem is symmetrical, which means the spheres have the same radii and move with equal translational and rotational velocities. In a more general case, i.e., when the particles have different radii and different velocities, the resistance coefficients (\hat{F}_i , \hat{T}_i) and consequently the forces and torques (F_i , T_i) acting on them are not identical.

III. RESULTS

A. Comparison of the force representations

In the step preceding the computation of the collision efficiency, a detailed comparison of different representations for the aerodynamic forces is made. The analysis concerns the relative motion of two spheres with equal and unequal radii. Two different cases are considered where the liquid spheres move at the same velocity in directions normal and parallel to the line connecting their centers. Figures 3–6 show interaction forces normalized by the Stokes drag acting on a single droplet for a wide range of normalized gap sizes, ξ .

Figure 3 shows the normalized drag force acting on an equal-sized pair of spheres moving with the same velocity in opposite directions along their line of centers. Such a comparison enables us to quantify distinctions in different formulations of aerodynamic forces, i.e., rigid particles under

continuum or noncontinuum lubrication, fluid drops, etc. The growth rate of each representation is shown next to the curves as $\xi \rightarrow 0$, that is, the slope of the line for small ξ . Similar to rigid spheres, the resistance coefficients for a pair of fluid drops at large viscosity ratios (blue lines) increase to infinity but the growth rate, $\xi^{-1/2}$, is slower at moderate viscosity ratios [18,25]. These rates for the limiting cases of highest and lowest viscosity ratios, $\hat{\mu}_r \rightarrow \infty$ and 0, approach ξ^{-1} and ~ 0 , respectively. The former is consistent with the solution that assumes a no-slip boundary condition on the surfaces of rigid spherical particles. The latter is quantitatively identical to the case of rigid particles under perfect slip (lower red dashed line) [37]. The noncontinuum lubrication force (red line) starts to deviate from both the continuum one (black dashed line) and the continuum-slip one (higher red dashed line) for $\xi < 10^{-1}$. For larger separation distances the differences are negligible. There are two key differences in the representation of the drag force for a noncontinuum flow in the gap. First, the growth rate as $\xi \rightarrow 0$ is weaker with $\hat{F} \propto \ln(\ln \xi^{-1})$ [19,23]. Second, the value of this lubrication force is smaller, and the reduction depends on the Knudsen number. In this study, the mean-free path is constant, and equal to $l_m = 0.1 \mu\text{m}$; therefore Kn is only a function of the size of the pair. In practice, the mean-free path is inversely proportional to the ambient pressure [41]. This dependence should be taken into account when modeling convective clouds, as the atmospheric pressure decreases with altitude.

The strict comparison of different formulations of aerodynamic interactions between a pair of typical cloud droplets, i.e., $a = O(10 \mu\text{m})$ and $\hat{\mu}_r = O(100)$, has been made with a rigid pair under no slip. The comparison reveals that the noncontinuum effect has a much stronger influence on the reduction of lubrication forces than the mobility of interfaces of liquid particles. In other words, although each effect noticeably impacts lubrication forces, a combined description of both effects using the solution developed by Rother *et al.* [6] would be close to the continuum-slip one. Finally, the drag forces approximated by the ISM for two limits of viscosity ratio are shown. The two purple lines in Fig. 3 represent the interacting force for a rigid pair, i.e., when $\hat{\mu}_r \rightarrow \infty$ (rigid particle limit) and for a fluid pair with $\hat{\mu}_r = 0$ (inviscid bubble limit). Both functions flatten for $\xi < 10^{-2}$ suggesting that under the ISM, it is not feasible to accurately represent the short-range lubrication. Note that the resistances with $\hat{\mu}_r = 0$ are presented only to show the limit of each representation, but they are not relevant to cloud droplets.

Figure 4 shows the normalized drag acting on two approaching rigid particles and quantify the differences resulting from considering the noncontinuum effects. These drag forces are evaluated for a system with two equal-sized spheres at different Knudsen numbers, corresponding to different radii. The curves compare the standard solutions that assume continuity of the medium (black line) to those with noncontinuum assumptions. The continuum-slip resistance (green dashed lines) is derived analytically assuming continuity of flow in the gap and having a Maxwell slip boundary condition on particle surfaces. In the calculations we used $l_m = 0.1 \mu\text{m}$ and $C_m = 1$ [42]. This representation is valid when the gap is much larger than the mean-free path of air molecules, and hence is limited to small Knudsen numbers ($Kn < 0.1$). In addition, noncontinuum lubrication force (red lines) evaluated analytically at different noncontinuum regimes (including slip-flow) is shown, which is also valid at large Kn . The comparison shows how the noncontinuum effects change the drag acting on rigid particles. For large separation distances the noncontinuum representation [19,23] agrees well with the continuum-slip solution of Reed and Morrison [37], because the noncontinuum lubrication of Sundararajakumar and Koch [19] considers the slip flow for gaps much larger than the mean-free path of molecules. Furthermore, all representations are identical in the limit $Kn = 0$ for the entire range of the normalized gap. For small separations, however, the noncontinuum lubrication deviates from the continuum-slip representation especially at larger Kn . Figure 5 presents the normalized drag acting on a pair of spheres moving in the same direction parallel to the line of centers. As expected the force representation for a pair of fluid drops with $\hat{\mu}_r \rightarrow \infty$ is the same as that of rigid spheres without slip under the continuum assumption. A reduction in the viscosity ratio of a fluid pair enhances the drag until the limit $\hat{\mu}_r = 0$. In this extreme case, the interactions between liquid particles and rigid particles under perfect slip are identical.

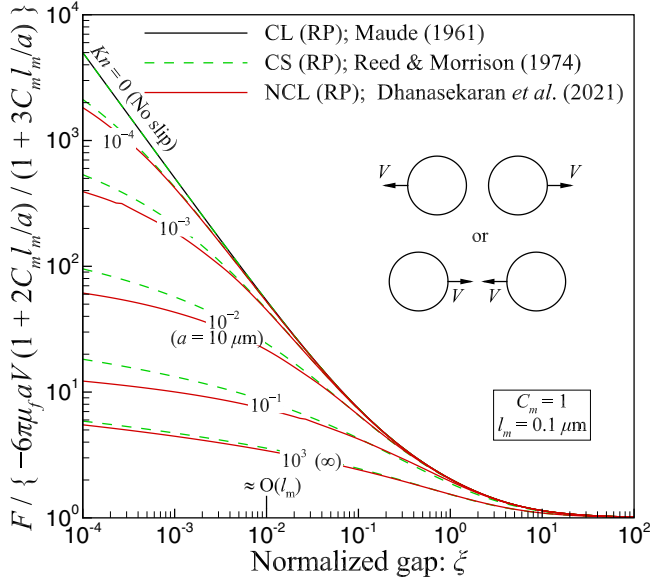


FIG. 4. Comparison of drag forces acting on two rigid spheres that move along the line connecting their centers. The forces were evaluated at different Kn using two different approaches: (1) continuum flow with slip boundary condition and (2) noncontinuum lubrication.

The approximate representations from the ISM are also presented at the same limits $\hat{\mu}_r \rightarrow \infty$ and 0, which can be compared with the exact representations (lower and higher blue lines, respectively).

In this study, depending on Kn of each pair, the noncontinuum effects for this type of motion is handled using the continuum-slip resistances of Reed and Morrison [37] since, as mentioned, the solution by Dhanasekaran *et al.* [23] has been developed for an opposing orientation. When

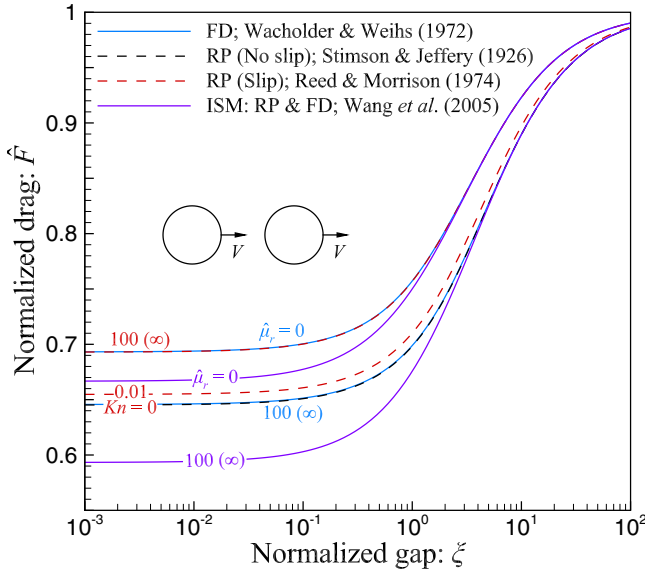


FIG. 5. The drag acting on a pair of spheres translating in the same direction along their line of centers.

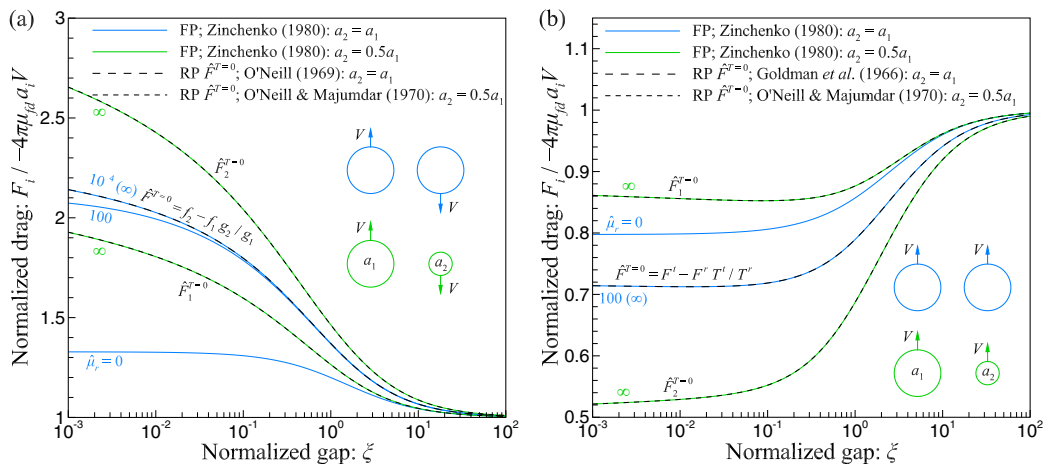


FIG. 6. Comparison of the normalized drag acting on a pair of spheres translating normal to their line of centers in (a) an opposing or (b) the same direction. The two expressions for $\hat{F}^{T=0}$ follow the notations in each corresponding study.

computing the collision efficiency of cloud droplets, this case is of particular importance. Small differences in the lubrication forces may result in large variations in E_{12} . The reason is that the velocity at which the droplets follow each other is relatively large and roughly proportional to their terminal velocities. In the former case, i.e., squeezing flow, the relative velocities are definitely smaller and proportional to the differences in the terminal velocities.

Further analysis concerns aerodynamic interactions of particles moving normal to their line of centers. Figures 6(a) and 6(b) show the normalized drag acting on two equal and nonequal spheres moving in an opposite and the same direction, respectively. For a pair of fluid drops with equal radii (blue lines), the drags change with the viscosity ratio until reaching their limits. At this extreme value, the drag has an identical representation as the drag acting on a pair of freely rotating rigid spheres (black long-dashed line) [27]. The expressions for $\hat{F}^{T=0}$ shown in Fig. 6 are the same as Eq. (17). The notations differ because they are adopted from the corresponding studies by Goldman *et al.* [39] and O'Neill [40].

The drag force at the limit of high viscosity ratio is additionally presented for spheres with unequal radii (green lines). The representations are also in accord with the net forces acting on an unequal pair of freely rotating rigid spheres (black short-dashed lines). For the comparison we used the solution developed by Zinchenko [27].

B. Collision efficiency

The collision efficiency computed using different representations of aerodynamic forces discussed above is presented in Figs. 7(a)–7(c). Three panels correspond to simulations with different radii of the larger droplets: $a_1 = 10, 20, 30 \mu\text{m}$. The radius of the smaller droplet depends on the parameter λ specified on the horizontal axis. The effects of droplet inertia, radii ratio, and van der Waals force have already been discussed in several former studies [13,20,21]. Accordingly, van der Waals forces are not taken into consideration in the present simulations. Here the main focus is on the impact of noncontinuum lubrication and internal circulation of the water inside droplets (fluid pairs with mobile interfaces). The reference E_{12} has been computed for a pair of rigid spheres under the continuum flow assumption using two different force representations: (1) resistance functions of Jeffrey and Onishi [34] and (2) solutions in bispherical coordinates of Stimson and Jeffery [35] and O'Neill and Majumdar [36]. Both methods give similar results, and the difference is much less than 1%. Therefore, in Figs. 7(a)–7(c), only the results from the Jeffrey and Onishi [34] representation are

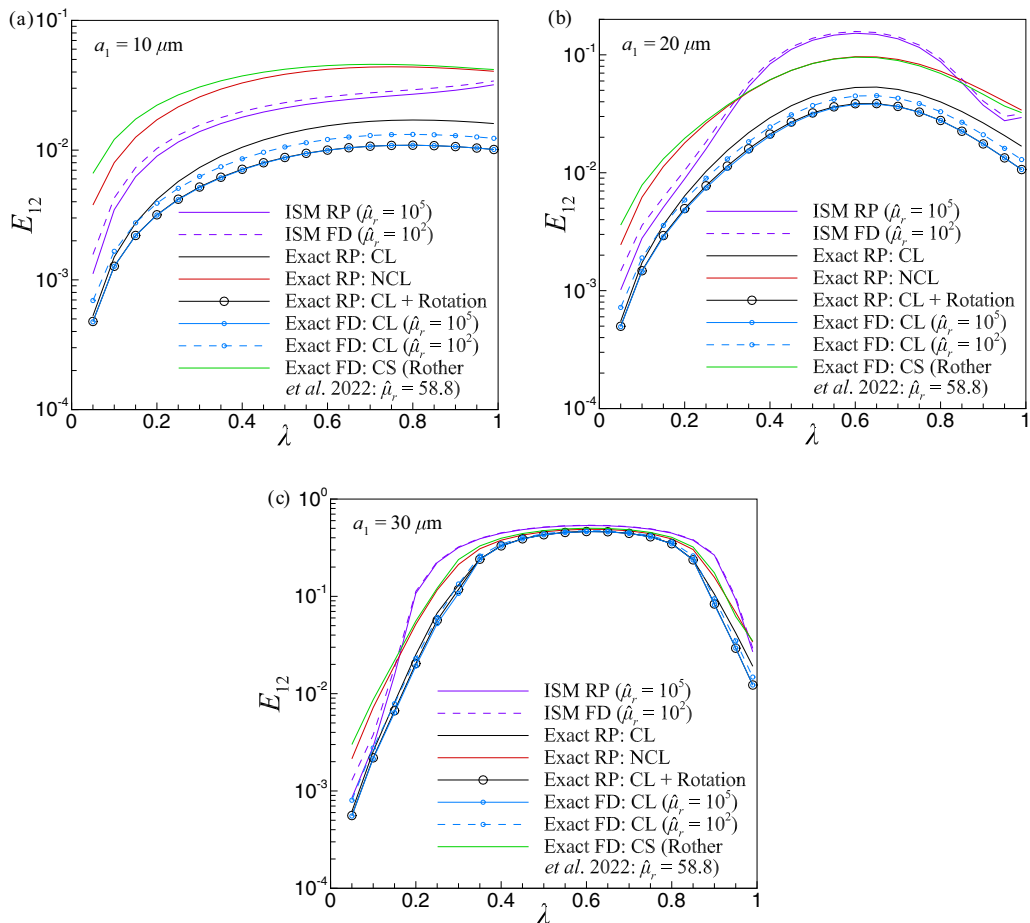


FIG. 7. Collision efficiency as functions of radii ratio under various force representations.

shown (black solid line), marked with “Exact RP: CL.” The raw numerical data are also tabulated in Appendix C in Tables II, III, and IV. In all three panels, E_{12} computed under the exact force representation (black solid line) agrees well with results of Hocking and Jonas [20] (Fig. 3 therein). Also, E_{12} evaluated using the ISM for a rigid pair matches well the data in Wang *et al.* [15] (Fig. 8 and Table 5 therein). A slight discrepancy is, among other factors, due to the different definitions for the collision gap. A common method to avoid the problem of drag singularity is a tiny enlargement of the collision radius. This is usually done by increasing the radius of the *larger* particle, such that the new collision radius is $R_{\text{col}} = R + \epsilon_{\text{col}} a_1$ [15,20,21]. However, in the present study the minimum separation distance below which the collision is assumed is a fraction of the *average* radius: $R_{\text{col}} = R(1 + \frac{1}{2}\xi_{\text{col}})$ where $\xi_{\text{col}} = 10^{-3}$.

The colors, marks, and patterns of curves are chosen to make comparison more convenient. The purple lines represent E_{12} computed using the ISM. Black and blue correspond to the models for rigid particles and fluid drops, respectively. The blue lines are marked with circles to be compared with the circle-marked black line that takes the rotation of rigid particles, Eq. (7), into consideration. The red line marks the simulations that account for the noncontinuum effects in lubrication forces. The green line shows a particular case from the reference data of Rother *et al.* [6] in which the van der Waals forces are excluded. As such, the data can be fairly compared with the models utilized here. These collision efficiencies are computed using a model through which the

TABLE I. List of misprints found in the studies on two-sphere problem.

Study	Equation	Misprinted form	Corrected form	Description
Stimson and Jeffery [35]	(37)	$\frac{2}{3}$	$\frac{4}{3}$	Refs. [17,49,50]
Maude [17]	F_1 and F_2	$(A_n \mp B_n + C_n \mp D_n)$	$(A'_n \pm B'_n + C'_n \pm D'_n)$	Goddard <i>et al.</i> [50] provided the correct form. Also, computational tests based on cross-comparison of the factors with their counterparts in Stimson and Jeffery [35].
	$\Delta B'_n$	$[-4 \exp(n + \frac{1}{2})(\alpha - \beta) \cdots + \cdots \cosh(\alpha - \beta)]$	$\{-4 \exp[-(n + \frac{1}{2})(\alpha - \beta)] \cdots + \cdots \cosh(\alpha + \beta)\}$	
	$\Delta C'_n$	$[\cdots \sinh(n + \frac{3}{2})(\alpha - \beta) - \cdots \sinh(n + \frac{1}{2})(\alpha - \beta) \times \sinh(n + \frac{1}{2})(\alpha - \beta) \cdots]$	$[\cdots \sinh(n + \frac{3}{2})(\alpha + \beta) - \cdots \sinh(n + \frac{1}{2})(\alpha + \beta) \times \sinh(n + \frac{1}{2})(\alpha + \beta) \cdots]$	
	$\Delta D'_n$	$[\cdots \sinh(n + \frac{1}{2})(\alpha + \beta) \cdots]$	$[\cdots \sinh(n + \frac{1}{2})(\alpha - \beta) \cdots]$	
O'Neill and Majumdar [36]	(5.10)	$\sinh^2 \beta $	$\sinh^3 \beta $	Torque: $G_\Omega \propto b^3$
Wacholder and Weihs [38]	(2.46): last factor	$(2n - 1)$	$(2n + 1)$	^a Ref. [35]; computational tests compared with Table 1 therein [38]
Haber <i>et al.</i> [26]	[32] and [33] [C-7] [B-8]	c $\delta_3 = 2(2n + 1)^2$ $-C_n^\alpha e^{(n+3/2)\alpha}$	c^2 $\delta_3 = -2(2n + 1)^2$ $+C_n^\alpha e^{-(n+3/2)\alpha}$	Zinchenko [28]; note: $c = a \sinh(\alpha)$ Zinchenko [28] Cross-comparison of the systems of equations in Ref. [38] [third line of (2.30)] and in Ref. [26]; computational tests
Reed and Morrison [37]	(20): last line	$\mp n(n + 1)$	$\pm n(n + 1)$	Cross-comparison with (26) in Stimson and Jeffery [35]
Beshkov <i>et al.</i> [51]	[1]: last line	$\{\cdots - (2n - 1) \sinh 2\alpha\}$	$\{\cdots - (2n + 1) \sinh 2\alpha\}$	Section III.C in Ref. [18], Sec. 9.4.3 in Ref. [31], and (B-12) in Ref. [26]
Kim and Karrila [31]	[3] (9.39): $N_1^{(n)}$	$K_n = \frac{n(n+1)}{(2n+2)(2n-1)}$ $-2(2n + 1) \sinh 2\alpha$	$K_n = \frac{n(n+1)}{(2n+3)(2n-1)}$ $+2(2n + 1) \sinh 2\alpha$	^b Ref. [17]; computational tests compared with Refs. [26,51].
Jeffrey and Onishi [34]	(4.9)	$P_{s(q-s)(p-n+1)}$	$P_{s(q-s)(p-n-1)}$	Refs. [21,52,53]
	(6.12)	f_{2j}	f_{2k}	Ichiki [53]
	(6.13)	$\{\cdots \frac{\lambda^2}{1+\lambda}\}$	$\underbrace{-\frac{16\lambda^2}{(1+\lambda)^4}}_{\text{missing term}} \cdots \{\cdots \underbrace{\frac{\lambda^2}{4(1+\lambda)}}_{\text{correction}}\}$	

TABLE I. (Continued.)

Study	Equation	Misprinted form	Corrected form	Description
	(7.10): g_4	$\frac{4}{5} \frac{\lambda^2}{(1+\lambda)^4}$	$\frac{\lambda^2}{10(1+\lambda)}$	Table 11.5 in Kim and Karrila [31]
	(7.10): g_5	$\frac{4}{125} \frac{\lambda(43-24\lambda+43\lambda^2)}{(1+\lambda)^4}$	Ref. [31]: $\frac{1}{250} \frac{\lambda(43-24\lambda+43\lambda^2)}{(1+\lambda)}$ Ref. [54]: $\frac{2}{125} \frac{\lambda(43-24\lambda+43\lambda^2)}{(1+\lambda)^4}$ Ref. [53]: $\frac{1}{125} \frac{\lambda(43-24\lambda+43\lambda^2)}{(1+\lambda)^4}$	Computational tests show Ichiki [53] suggestion better approximates g_{11} and g_{12} of O'Neill and Majumdar [36].
Goddard <i>et al.</i> [50]	(60)	$\frac{n+1}{2n+3}$	$\frac{n+2}{2n+3}$	Printed correctly in (C35) therein [50]. Also, (3.45) in Ref. [39].
Rother <i>et al.</i> [6]	(A.11)	$e^{-\frac{(n+3/2)\eta_1}{2n+3}} - e^{-\frac{(n-1/2)\eta_1}{2n-1}}$	$\frac{e^{-(n+3/2)\eta_1}}{2n+3} - \frac{e^{-(n-1/2)\eta_1}}{2n-1}$	Printed correctly in Ref. [55].
	(A.12)	$e^{-\frac{(n+3/2)\eta_2}{2n+3}} - e^{-\frac{(n-1/2)\eta_2}{2n-1}}$	$\frac{e^{(n+3/2)\eta_2}}{2n+3} - \frac{e^{(n-1/2)\eta_2}}{2n-1}$	
	(A.14)	$E_{n-1} e^{-(n-3/2)(\eta_2)}$	$E_{n-1} e^{-(n-3/2)(\eta_2 - \eta_1)}$	Computational tests compared with Refs. [26,37]
	(A.14)	$E_n e^{-(n-1/2)(\eta_2)}$	$E_n e^{-(n-1/2)(\eta_2 - \eta_1)}$	
	(A.14)	$\frac{(n+1/2)^2 e^{-(n+1/2)\eta_2}}{2n+1}$	$\frac{(n+1/2)^2 e^{(n+1/2)\eta_2}}{2n+1}$	
	(A.15)	$F_i =$	$F_i = -4\pi \mu_e c \sum f(n, \eta_i)$	
	and	$-4\sqrt{2}\pi \mu_e / c \sum f(n, \eta_i)$		
	(A.16)			

^aFor very large viscosity ratios the solution for a fluid drop ($\sigma \rightarrow \infty$ in Ref. [38]) approaches that of a rigid particle (λ in Ref. [35]). A careful comparison at this limit shows the factor is misprinted.

^bFor very large viscosity ratios the solution for a fluid drop ($\lambda \rightarrow \infty$ in Ref. [31]) approaches that of a rigid particle (λ_2 in Ref. [17]). A careful comparison at this limit shows the factor is misprinted.

internal circulation and noncontinuum effects (within free-slip regime) are jointly accounted for. The differences between the rigid particles and fluid drops are manifested using different values of the viscosity ratio, which are $\hat{\mu}_r = 10^5$ and 10^2 , correspondingly. The latter corresponds to the water droplets in air under typical conditions of atmospheric clouds. The black line with circle symbols is the only case in which the rotation of rigid pairs, Eq. (7), is considered. Based on the obtained results, noticeable differences in E_{12} are observed only for the droplets with low inertia (the two cases for $a_1 = 10$ and $20 \mu\text{m}$). For larger droplets, different force representation models predict similar values for the collision efficiency.

The approximate force representation obtained from the ISM does not capture the singularity of the lubrication forces [see Fig. 7(a) in Ref. [15]]. Therefore, the resistance remains finite when the gap between the droplets goes to zero. This allows us to compute E_{12} even without employing the collision gap model, i.e., $R_{\text{col}} = a_1 + a_2$. The differences in the collision efficiency between the rigid particles and fluid drops (solid vs dashed purple line) are clearly visible for $a_1 = 10 \mu\text{m}$. Overall, E_{12} of liquid drops is about 10% larger. This is due to the lower drag force acting on a single liquid sphere compared to the rigid one. In general, the ISM largely overestimates E_{12} when compared with the exact representation (purple vs blue lines).

Under exact force representations for a rigid pair, E_{12} is significantly larger when considering the noncontinuum lubrication (red vs black line). The relative increase due to noncontinuum effects is more pronounced for smaller droplets, on average $\approx 125\%$; see Fig. 7(a). For larger droplets this enhancement is about 25% [see Fig. 7(c)] since the higher inertia of these droplets has a stronger impact on collisions. The reason for the observed increase is the lower drag force acting on particles

TABLE II. Collision efficiency between pairs of $a_1 = 10 \mu\text{m}$ and $a_2 = \lambda a_1$. Values on the first and second lines of every row are computed considering a normalized collision gap of $\xi_{\text{col}} = 10^{-3}$ and 0 (marked with asterisk), respectively.

λ	ISM RP $\hat{\mu}_r = 10^5$	ISM FD $\hat{\mu}_r = 10^2$	Exact RP CL (JO)	Exact RP CL (Bi)	Exact RP NCL (JO)	Exact RP +Rot. (JO)	Exact RP +Rot. (Bi)	Exact FD $\hat{\mu}_r = 10^5$	Exact FD $\hat{\mu}_r = 10^2$
0.05	0.001113 0.001043*	0.001569 0.001494*	0.000528	0.000525	0.003776 0.003656*	0.000478	0.000475	0.000475	0.000693 0.000204*
0.1	0.003474 0.003348*	0.004283 0.004153*	0.001503	0.001503	0.008016 0.007850*	0.001273	0.001275	0.001272	0.001660 0.000490*
0.15	0.006236 0.006064*	0.007327 0.007151*	0.002751	0.002750	0.012567 0.012323*	0.002199	0.002199	0.002189	0.002749 0.000812*
0.2	0.008980 0.008770*	0.010298 0.010085*	0.004172	0.004179	0.017132 0.016814*	0.003173	0.003180	0.003158	0.003899 0.001157*
0.25	0.011544 0.011303*	0.013048 0.012803*	0.005729	0.005727	0.021547 0.021160*	0.004184	0.004184	0.004149	0.005080 0.001517*
0.3	0.013891 0.013624*	0.015547 0.015276*	0.007347	0.007338	0.025703 0.025252*	0.005196	0.005190	0.005142	0.006269 0.001890*
0.35	0.016021 0.015733*	0.017804 0.017512*	0.008962	0.008955	0.029522 0.029013*	0.006181	0.006176	0.006118	0.007441 0.002272*
0.4	0.017943 0.017637*	0.019832 0.019522*	0.010523	0.010523	0.032943 0.032383*	0.007118	0.007120	0.007056	0.008570 0.002654*
0.45	0.019660 0.019340*	0.021638 0.021313*	0.011986	0.011993	0.035923 0.035315*	0.007990	0.007997	0.007933	0.009625 0.003029*
0.5	0.021174 0.020842*	0.023224 0.022887*	0.013309	0.013320	0.038430 0.037780*	0.008774	0.008784	0.008725	0.010578 0.003401*
0.55	0.022489 0.022146*	0.024596 0.024249*	0.014457	0.014471	0.040451 0.039763*	0.009451	0.009463	0.009412	0.011403 0.003675*
0.6	0.023616 0.023265*	0.025767 0.025412*	0.015405	0.015420	0.041987 0.041265*	0.010006	0.010019	0.009977	0.012083 0.003641*
0.65	0.024579 0.024222*	0.026763 0.026402*	0.016140	0.016154	0.043053 0.042297*	0.010430	0.010441	0.010410	0.012605 0.003985*
0.7	0.025417 0.025056*	0.027624 0.027259*	0.016657	0.016670	0.043672 0.042886*	0.010719	0.010729	0.010708	0.012966 0.004149*
0.75	0.026188 0.025823*	0.028409 0.028041*	0.016962	0.016973	0.043879 0.043065*	0.010875	0.010884	0.010870	0.013167 0.004246*
0.8	0.026966 0.026597*	0.029197 0.028825*	0.017067	0.017077	0.043716 0.042874*	0.010907	0.010915	0.010906	0.013220 0.004265*
0.85	0.027847 0.027477*	0.030084 0.029710*	0.016992	0.017000	0.043226 0.042358*	0.010825	0.010832	0.010827	0.013136 0.004224*
0.9	0.028948 0.028576*	0.031186 0.030812*	0.016759	0.016766	0.042458 0.041564*	0.010643	0.010649	0.010646	0.012934 0.004133*
0.95	0.030399 0.030028*	0.032632 0.032258*	0.016394	0.016401	0.041458 0.040539*	0.010377	0.010382	0.010384	0.012631 0.004000*
0.99	0.031904 0.031535*	0.034125 0.033753*	0.016024	0.016031	0.040524 0.039585*	0.010113	0.010118	0.010114	0.012329 0.003869*

in squeezing flow. For two closely spaced rigid spheres approaching with equal velocities, the repulsive aerodynamic force evaluated under the continuum assumption is inversely proportional to the separation gap, i.e., $\hat{F} \propto \xi^{-1}$. However, if the noncontinuum effects are accounted for, the drag takes a sluggish logarithmic growth, i.e., $\hat{F} \propto \ln(\ln \xi^{-1})$ [19,23]. This estimate quantifies the dependency between lower drag and higher probability of collisions. Moreover, the results of Rother

TABLE III. Collision efficiency between pairs of $a_1 = 20 \mu\text{m}$ and $a_2 = \lambda a_1$. Values on the first and second lines of every row are computed considering a normalized collision gap of $\xi_{\text{col}} = 10^{-3}$ and 0 (marked with asterisk), respectively.

λ	ISM RP $\hat{\mu}_r = 10^5$	ISM FD $\hat{\mu}_r = 10^2$	Exact RP CL (JO)	Exact RP CL (Bi)	Exact RP NCL (JO)	Exact RP +Rot. (JO)	Exact RP +Rot. (Bi)	Exact FD $\hat{\mu}_r = 10^5$	Exact FD $\hat{\mu}_r = 10^2$
0.05	0.001016 0.000947*	0.001468 0.001394*	0.000550	0.000547	0.002446 0.002347*	0.000499	0.000496	0.000495	0.000721 0.000220*
0.1	0.002785 0.002663*	0.003577 0.003449*	0.001728	0.001728	0.006207 0.006019*	0.001475	0.001476	0.001460	0.001897 0.000577*
0.15	0.005087 0.004915*	0.006202 0.006023*	0.003611	0.003609	0.011288 0.010995*	0.002932	0.002931	0.002859	0.003570 0.001115*
0.2	0.008881 0.008644*	0.010459 0.010213*	0.006370	0.006380	0.017899 0.017497*	0.004962	0.004973	0.004808	0.005872 0.001892*
0.25	0.015892 0.015555*	0.018221 0.017875*	0.010261	0.010257	0.026271 0.025749*	0.007749	0.007747	0.007439	0.008987 0.002993*
0.3	0.029692 0.029227*	0.033148 0.032684*	0.015433	0.015413	0.036512 0.035855*	0.011410	0.011394	0.010916	0.013107 0.004513*
0.35	0.053900 0.053365*	0.058371 0.057839*	0.021875	0.021857	0.048407 0.047595*	0.015975	0.015961	0.015319	0.018322 0.006529*
0.4	0.083581 0.083025*	0.088578 0.088026*	0.029291	0.029292	0.061222 0.060242*	0.021286	0.021289	0.020526	0.024465 0.009027*
0.45	0.111261 0.110697*	0.116508 0.115948*	0.037024	0.037049	0.073750 0.072600*	0.026907	0.026931	0.026110	0.031013 0.011847*
0.5	0.132948 0.132378*	0.138326 0.137756*	0.044149	0.044191	0.084583 0.083277*	0.032148	0.032189	0.031389	0.037151 0.014721*
0.55	0.146926 0.146348*	0.152368 0.151791*	0.049694	0.049744	0.092442 0.091008*	0.036232	0.036281	0.035558	0.041982 0.016884*
0.6	0.152441 0.151857*	0.157926 0.157342*	0.052880	0.052931	0.096407 0.094882*	0.038501	0.038549	0.037967	0.044761 0.017297*
0.65	0.149126 0.148536*	0.154632 0.154043*	0.053282	0.053328	0.096040 0.094465*	0.038591	0.038634	0.038226	0.045065 0.018001*
0.7	0.136792 0.136197*	0.142286 0.141693*	0.050902	0.050940	0.091447 0.089867*	0.036522	0.036558	0.036323	0.042878 0.017154*
0.75	0.115674 0.115074*	0.121072 0.120476*	0.046176	0.046206	0.083281 0.081746*	0.032690	0.032718	0.032613	0.038596 0.015303*
0.8	0.087475 0.086878*	0.092571 0.091978*	0.039897	0.039920	0.072688 0.071240*	0.027760	0.027781	0.027748	0.032946 0.012796*
0.85	0.058084 0.057521*	0.058084 0.061855*	0.033036	0.033053	0.061124 0.059786*	0.022498	0.022513	0.022501	0.026813 0.010107*
0.9	0.037367 0.036899*	0.040560 0.040088*	0.026456	0.026468	0.050024 0.048776*	0.017560	0.017571	0.017559	0.021010 0.007604*
0.95	0.027620 0.027235*	0.030036 0.029646*	0.020676	0.020685	0.040385 0.039159*	0.013366	0.013373	0.013366	0.016090 0.005494*
0.99	0.029409 0.029038*	0.031650 0.031276*	0.016775	0.016782	0.033967 0.032702*	0.010641	0.010646	0.010652	0.012936 0.004130*

et al. [6] follow a similar trend to the results computed using the noncontinuum lubrication model (green vs red line). The resemblance is mainly due to the noncontinuum lubrication effects, whereas the differences are caused by two important factors. First, Rother *et al.* [6] developed a solution for a pair of fluid drops (having internal circulations with mobile interfaces), while Dhanasekaran *et al.* [23] considered rigid particles. Second, in each study noncontinuum lubrication has been quantified

TABLE IV. Collision efficiency between pairs of $a_1 = 30 \mu\text{m}$ and $a_2 = \lambda a_1$. Values on the first and second lines of every row are computed considering a normalized collision gap of $\xi_{\text{col}} = 10^{-3}$ and 0 (marked with asterisk), respectively.

λ	ISM RP $\hat{\mu}_r = 10^5$	ISM FD $\hat{\mu}_r = 10^2$	Exact RP CL (JO)	Exact RP CL (Bi)	Exact RP NCL (JO)	Exact RP +Rot. (JO)	Exact RP +Rot. (Bi)	Exact FD $\hat{\mu}_r = 10^5$	Exact FD $\hat{\mu}_r = 10^2$
0.05	0.000849	0.001288	0.000616	0.000612	0.002141	0.000559	0.000555	0.000553	0.000803
	0.000782*	0.001215*			0.002043*				0.000252*
0.1	0.002862	0.003775	0.002557	0.002557	0.007195	0.002191	0.002192	0.002146	0.002767
	0.002727*	0.003629*			0.006966*				0.000904*
0.15	0.015507	0.018573	0.008129	0.008123	0.019484	0.006673	0.006670	0.006376	0.007876
	0.015109*	0.018167*			0.019037*				0.002770*
0.2	0.107644	0.112581	0.025201	0.025241	0.051756	0.020400	0.020440	0.019239	0.023015
	0.107168*	0.112111*			0.050880*				0.008787*
0.25	0.222144	0.227092	0.067370	0.067352	0.116251	0.056775	0.056761	0.052499	0.060435
	0.221650*	0.226594*			0.114833*				0.026061*
0.3	0.317356	0.322077	0.130523	0.130462	0.212516	0.117738	0.117680	0.107228	0.134055
	0.316837*	0.321537*			0.206797*				0.059394*
0.35	0.390764	0.395222	0.241510	0.241508	0.308401	0.240997	0.240994	0.239501	0.260117
	0.390175*	0.394633*			0.304470*				0.129763*
0.4	0.445446	0.449659	0.330729	0.330730	0.377593	0.330135	0.330135	0.328469	0.344289
	0.444818*	0.449024*			0.374497*				0.257562*
0.45	0.484926	0.488974	0.390757	0.390758	0.426780	0.390139	0.390140	0.388504	0.401614
	0.484278*	0.488327*			0.424117*				0.337576*
0.5	0.511876	0.515793	0.430388	0.430389	0.460269	0.429763	0.429763	0.428232	0.439784
	0.511204*	0.515125*			0.457836*				0.389156*
0.55	0.528051	0.531920	0.454236	0.454237	0.480699	0.453600	0.453600	0.452194	0.462905
	0.527385*	0.531237*			0.478375*				0.420508*
0.6	0.534466	0.538306	0.464542	0.464543	0.489438	0.463884	0.463884	0.462602	0.473000
	0.533782*	0.537620*			0.487138*				0.433297*
0.65	0.531163	0.535047	0.461830	0.461831	0.486734	0.461132	0.461133	0.459969	0.470534
	0.530478*	0.534358*			0.484366*				0.430496*
0.7	0.517313	0.521313	0.444888	0.444889	0.471551	0.444129	0.444130	0.443083	0.454383
	0.516629*	0.520625*			0.469017*				0.410492*
0.75	0.490736	0.494925	0.409990	0.409991	0.441087	0.409144	0.409145	0.408231	0.421133
	0.490065*	0.494252*			0.438201*				0.367350*
0.8	0.447010	0.451491	0.348424	0.348426	0.389292	0.347484	0.347484	0.346751	0.362956
	0.446360*	0.450837*			0.385660*				0.283840*
0.85	0.377523	0.382419	0.238258	0.238261	0.303018	0.237326	0.237329	0.236880	0.260695
	0.376893*	0.381788*			0.297531*				0.146255*
0.9	0.265307	0.270729	0.105428	0.105457	0.157098	0.083491	0.083520	0.081787	0.094562
	0.264701*	0.270124*			0.154204*				0.043987*
0.95	0.092923	0.098103	0.042087	0.042105	0.068297	0.029331	0.029348	0.029390	0.034852
	0.092322*	0.097506*			0.066244*				0.013722*
0.99	0.026878	0.029222	0.019110	0.019117	0.033859	0.012263	0.012263	0.012272	0.014809
	0.026502*	0.028829*			0.032322*				0.004941*

in a different manner. To do so, Rother *et al.* [6] imposed slip boundary condition on drop surfaces while assuming a continuous flow in the gap between droplets. This is accurate at low Kn as long as the gap is much larger than the mean-free path of the flow. On the other hand, Dhanasekaran *et al.* [23] used several solutions obtained within various noncontinuum regimes, which is valid at high Kn and for gaps smaller than the mean-free path of air molecules. Furthermore, it is worth adding that the less steep increase in the noncontinuum lubrication forces enables performing simulations

without having to use the collision gap model. This leads to a small ($\approx 2\%$) decrease in E_{12} (see Tables II–IV in Appendix C).

The next set of results, shown in Figs. 7(a)–7(c) using the circle-marked black line, presents E_{12} computed in simulations that account for rotation of rigid particles. These values are in accord with E_{12} for liquid particles with $\hat{\mu}_r = 10^5$ (solid circle-marked blue line). This is an important finding viewing the fact that two different sets of problems yield the same results. An unavoidable consequence of considering particle rotation is the significant increase of the computational complexity. Accounting for rotational motion requires the calculation of more quantities including torques, angular velocities, additional resistance functions (defining the coupling between translational and rotational motion), and modified drag forces. The ordinary differential equation governing the angular velocity of rigid particles, Eq. (7), must be solved together with the equation for the translational velocity. All these factors remarkably enhance the computational time compared to the case in which rotation is neglected. As for the spherical drops, an equation for the angular momentum does not need to be solved since a rigid-body rotation is not defined for the internal flows circulating inside the droplets and the external torques acting on the droplets are zero. Thus, the computational time is much shorter, while values of E_{12} are in a quantitative agreement with those for the freely rotating rigid particles. The obtained results are consistent with the theory developed by Zinchenko [27]. According to hypotheses formulated there, the forces acting on two liquid particles with a very large $\hat{\mu}_r$ translating *normal* to their line of centers, are equal to those due to the translation of freely rotating rigid particles (see Fig. 6). It is also worth adding that the forces acting on two fluid drops of large $\hat{\mu}_r$ translating *along* their line of centers [26,38] are similar to those of rigid particles [17,34,35]. For the problem considered here, the conditions guaranteeing the free rotation are satisfied, because (1) the initial condition imposed is $\Omega_i = 0$ and (2) there are no external torques acting on the droplets.

In Figs. 7(a) and 7(b), comparison between rotating (circle-marked black line) and purely translating (regular black line) rigid pairs demonstrates that when the particles are allowed to rotate E_{12} declines roughly by 10% to 30% as λ increases from the smallest to largest values. Rotation, via the coupling terms in the resistance matrix, modifies the net drag acting on the pair normal to the line of centers, thereby reducing the chance of collision. For a pair of water droplets in still air, the viscosity ratio is of the order of $\hat{\mu}_r = 10^2$. Under such conditions, the collision efficiency of water droplets (blue dashed line) is larger than that for freely rotating rigid particles of the same density or liquid particles at $\hat{\mu}_r = 10^5$. This enhancement is from $\approx 20\%$ for almost equal-sized ($\lambda \rightarrow 1$) pairs to $\approx 45\%$ for the smallest radii ratio considered here ($\lambda = 0.05$). Again, the reason for the increase in E_{12} is the lower drag force acting on the approaching particles. We should be aware, however, that the comparison with purely translating rigid pairs (regular black line) is somehow biased because the interfaces (between drops' internal and external flows) of droplets are mobile.

Another comparison concerns the results obtained by employing exact and approximate (evaluated through the ISM) representations of aerodynamic interactions. One would expect that since the ISM yields a much smaller drag (at short separation distances) than noncontinuum lubrication (see Fig. 3), E_{12} under the ISM has to be always larger. It turns out, however, that in many cases the trend is opposite [see Figs. 7(a) and 7(b)]. The reason can be explained by considering a simplified example. For a pair of cloud droplets of radii ratio $\lambda = 0.7$, the terminal velocity of the smaller droplet is approximately half (since $\tau_i \propto a_i^2$) of the larger one. If aerodynamic interactions were neglected, the pair would maintain the same terminal velocities while settling under gravity. In Fig. 8 these terminal velocities are decomposed (see Fig. 1 in Rosa *et al.* [21]) into two elementary cases of the pair approaching and following at the same velocity. The first case on the r.h.s., based on exact solutions, is subjected to the singular resistances which prevent collision unless the collision gap model is utilized. For this case, a stronger drag reduces E_{12} . The second case on the r.h.s. is also important for this problem since a major contribution to total velocity is due to the pair following each other along gravity. (The least effective cases would be related to the horizontal components of velocities, being zero here, since they would be much smaller than settling velocities if aerodynamic interaction were considered.) For the second case, slight variations in the drag forces significantly

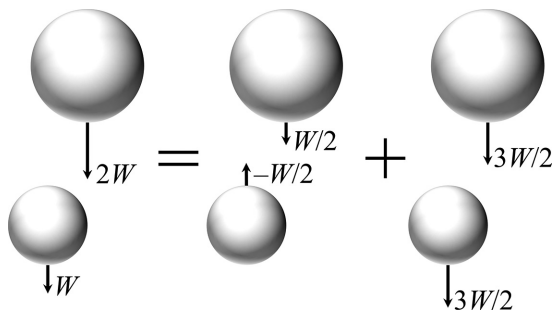


FIG. 8. Decomposition of velocity of an arbitrary two-body system with $\lambda = 0.7$ into two elementary and symmetrical cases.

change E_{12} in such a way that, contrary to the first case, a stronger drag leads to a larger E_{12} . The force from the ISM for the second case (following droplets) is compared with the noncontinuum representation in Fig. 5, exhibiting a weaker drag that tends to diminish E_{12} . This was neglected by the argument above which considers only the first case (approaching droplets). As such, the counterbalancing effect of approaching and following drags on collision efficiency leads not only to a larger E_{12} but sometimes also to a smaller one.

Finally, we examine the effect of the collision gap size on E_{12} under different representations of aerodynamic interactions. The aim is to check the possibility of collision using solely the models examined in this study, that is, without additional treatments such as collision gap model or van der Waals forces even though they strongly dominate the interaction between droplets at such small gaps. Therefore, the collision gap has to approach zero, and such simulations are a numerically challenging, especially for small λ . In all simulations discussed above the collision gap size was fixed and equal to $\xi_{\text{col}} = 10^{-3}$. This set of simulations is performed for $10^{-8} \leq \xi_{\text{col}} \leq 10^{-3}$. Note that to obtain numerical convergence for smaller ξ_{col} , it is necessary to reduce the integration time step. Since we use an adaptive Runge-Kutta scheme, the size of Δt is not fixed but assessed dynamically by local error estimation.

Figure 9 shows the collision efficiency computed using the collision gap model at different ξ_{col} . To reduce the computational cost, all simulations have been performed for the same setting of a larger droplet radius $a_1 = 20 \mu\text{m}$ and $\lambda = 0.7$. Each curve represents a different model of aerodynamic interactions. As expected, the simulations employing the approximate ISM representations are almost insensitive to ξ_{col} . Similarly, a rigid pair under noncontinuum lubrication description yields a nonzero E_{12} due to a slow logarithmically increasing resistance. For the other four cases E_{12} decreases with ξ_{col} , which is the effect of the singularity in the resistance coefficients of approaching pairs under a continuum description. Consequently, for rigid particles with and without rotation (black lines) as well as fluid drops with a high viscosity ratio (solid blue line), $E_{12} \rightarrow 0$ as we shrink ξ_{col} . The exception here is a fluid pair with $\hat{\mu}_r = 10^2$, showing that the decrease in E_{12} levels out as ξ_{col} is reduced. This is a result of resistance being proportional to $\xi^{-1/2}$ at a moderate $\hat{\mu}_r$, as opposed to ξ^{-1} for the other three cases. Accordingly, for this force representation E_{12} can be quantified without making use of the collision gap model or van der Waals forces. Such values are computed and presented in Tables II–IV in Appendix C.

C. Numerical aspects

This section focuses on numerical aspects of conducted simulations, including techniques, developments, tools, observations, issues, and challenges. The motivation for this analysis is to check the applicability of different representations of aerodynamic interactions to perform complex simulations of the dynamics of many particles in turbulent flows.

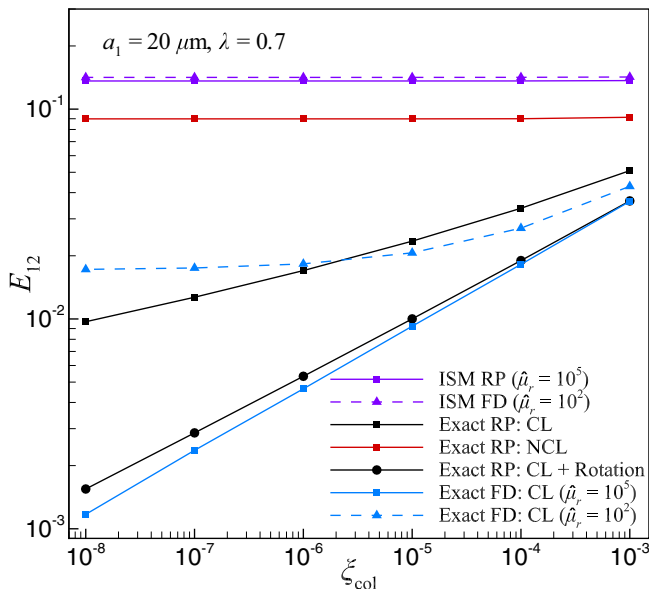


FIG. 9. Collision efficiency evaluated using different collision gaps.

1. Computation time

In terms of computational costs, the ISM features of relatively low complexity. Therefore, the results from the ISM are the fastest (seconds, in terms of wall-clock time) to obtain. At each time step the forces acting on the pair of droplets are computed by solving a small system of six equations that include three components of disturbance velocities at the location of each droplet. Computation time is much longer when employing exact representations of aerodynamic interactions [34] and the solutions in bispherical coordinates for rigid [35,36] or liquid [26,27] particles (minutes to hours). Rotation increases the computational cost (potentially by orders of magnitude depending on the problem) owing to the need for a much greater number of operations to calculate the forces, torques, coupling terms, and integrating two additional equations for the conservation of angular momentum, Eq. (7).

The convergence rate of computing the interaction forces using the solutions in bispherical coordinates or the multipole expansion of Jeffrey and Onishi [34] slows down as the gap between droplets decreases. It should be noted, however, that the second approach is easier to implement in computer codes and offers better computational performance. This desired feature (a faster convergence) was obtained by combining analytical solutions for nearly touching spheres with infinite series that define resistance coefficients for large separations. In all the simulations considered here, we found that the multipole expansion provides satisfactory accuracy even when summing the first 100 terms. To achieve similar precision by using the solutions in bispherical coordinates we need to sum up about 10^3 terms. Another factor influencing computational time is the particle radii ratio. For smaller λ , the calculation of aerodynamic interactions takes a longer time as more terms must be added up, so that the summations reach their limits. This applies in particular to the resistances given by O'Neill and Majumdar [36] for the motion of unequal particles in a direction perpendicular to their line of centers. Therefore, the smaller the radii ratio or spacing between the particles, the larger the system of equations to be solved. Moreover, for pairs with substantially different sizes the systems can be ill-conditioned. Another impact of the radii ratio on computation time comes from the differences in the settling speed. As $\lambda \rightarrow 1$, the pair approaches at a much slower relative velocity since $\Delta W \rightarrow 0$, so the first r.h.s. component in Fig. 8 diminishes. In this

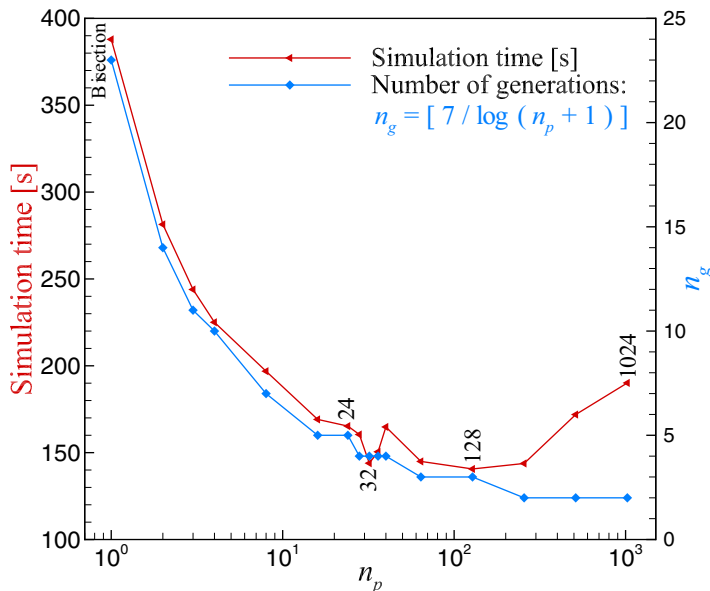


FIG. 10. Change in simulation time and number of generations with the number of processes in \log_{10} scale.

limit, the equations of motion must be integrated for longer periods of time to allow the particles to collide.

Apart from the aspects discussed above, the computation time is significantly influenced by the integration scheme. To solve the equations of motion, Eqs. (5)–(7), three different schemes were employed: (1) fourth-order Adams-Bashforth, (2) classical fourth-order Runge-Kutta, and (3) adaptive Runge-Kutta that dynamically adjusts Δt based on error estimations. All these schemes led to the same results. As expected, the best performance was achieved with the adaptive Runge-Kutta.

2. Algorithm parallelization

In the former study by Rosa *et al.* [21], the initial condition y_0 , i.e., the off-center horizontal separation, was successively modified (in subsequent generations) by making use of the standard bisection method. The entire range of collision efficiency $E_{12} \in [0, 1]$ was scanned until further divisions of the subrange did not show any significant change in E_{12} . Regrettably, such an approach features of a fairly low convergence rate.

A relatively simple remedy to speed up the computation is to parallelize the algorithm via the message passing interface (MPI) library. For this purpose, we adopt the idea that is based on the multithreaded bisection search. In the serial approach, the considered range that defines the collision efficiency is halved in subsequent generations, while in the parallel code the range of interest is divided by $n_p + 1$ where n_p is the number of processes (subgenerations performed with different initial aims) each given to a computational core. Computations in subsequent generations are carried out with the same number of processors but for a much narrower starting range than in the serial method. This significantly reduces the number of generations needed to obtain accurate results.

In Fig. 10 the left vertical axis refers to the change in the total simulation time (the wall clock time) for a set of 20 simulations carried with different number of processors, shown in \log_{10} scale, assuming $a_1 = 10 \mu\text{m}$ and $\lambda = 0.05$ to 0.99 . The right vertical axis shows the number of generations (n_g) required to narrow the initial range $[0, 1]$ to the desired accuracy of 10^{-7} in E_{12} . These measured quantities are plotted as a function of the number of processes. To achieve the accuracy, in subsequent n_g generations, the considered (narrowing) range was divided into $n_p + 1$

subranges in such a way that

$$\frac{1}{(n_p + 1)^{n_g}} \leq 10^{-7}. \quad (18)$$

Figure 10 demonstrates that both lines follow a similar monotonic trend up to $n_p = 128$. The reason for the decline in performance for $n_p > 128$ is that all subgenerations (processes) start simultaneously but do not finish at the same time. Note that each subsequent generation begins when all the processes of the previous generation are completed. Consequently, there is a certain idle time as the completed processes must wait for those that are still in progress. For a large n_p , there is a significant difference in simulation time between the fastest and slowest processes. This difference negatively impacts computing performance, especially in the early generations. On the other hand, the favorable performance obtained for $n_p \leq 128$ is a consequence of the higher scanning resolution. Since the machine we were using has 24-core processors, most of the simulations in this paper were performed at $n_p = 24$.

IV. CONCLUSIONS

This study quantifies the collision efficiency of two nondeformably spherical particles settling under gravity in quiescent air. The investigations were carried out by means of numerical simulations employing our in-house code. Most of the simulations were performed using settings characteristic for typical cloud droplets. An accurate description of this process finds an important application in numerical weather prediction systems. To test sensitivity of the numerical model, additional simulations at different relative viscosities were also performed. A number of cases were considered assuming different sizes and radii ratios of the particle pairs. The main focus, however, was on small droplets with radii in the range 0.5 to 30 μm .

The governing equation for particle motion includes various representations of the aerodynamic interaction. This is the main element that extends previous studies on this topic. The interacting forces and torques were evaluated using both an approximate method and exact solutions to the Stokes equation for two spheres. Other important effects analyzed here are related to the noncontinuum lubrication and internal circulation of the water inside droplets. The obtained results are compared with reference data available in the literature. The comparison shows that the collision efficiency computed using the approximate model (ISM) or the noncontinuum lubrication is usually larger than that of rigid particles moving in a continuous medium. In the considered range of parameters, the increase in E_{12} for the noncontinuum lubrication varies from 25% to 125%. As for the liquid particles, the collision efficiency is also enhanced compared to the rigid pair. This enhancement may reach even 45%. The reason for this increase resides in a somewhat lower drag acting on the settling spheres. In the case of liquid particles, the drag force is partially mitigated by the mobile interface. In general, noncontinuum lubrication has a larger impact on the collision efficiency compared to the internal circulation of drops, which loses its influence as their inertia (size) increases. In numerical simulations, therefore, treating medium-sized cloud droplets as rigid particles is a reasonable assumption, but considering noncontinuum effects in their aerodynamic interaction is expected to change the results. It also has been demonstrated that the collision efficiency of liquid particles with a very large viscosity ratio is the same as that of freely rotating rigid spheres of the same density.

The second part of this study deals with the numerical aspects. Computing the aerodynamic interactions comes with a huge computational cost. The numerical complexity is particularly problematic when using solutions in bispherical coordinates. It should be noted that these interactions have to be calculated at every time step for different separation distances and radii ratios. To speed up the computation, the code was parallelized using the MPI libraries. In this way, we were able to obtain results in a much shorter time and with greater accuracy.

This study is a step forward to model multi-particle systems in turbulent flows. Therefore, one potentially significant direction of future research is to implement different representations of

aerodynamic interactions in a code for hybrid direct numerical simulations. This paves the way for a more realistic modeling of cloud processes.

The code for computing hydrodynamic interaction is available online [43]. It was developed both to plot the figures in this study and to calculate forces and torques in the equations of motion. The resistance functions were taken from the research web page of David Jeffrey [44].

ACKNOWLEDGMENTS

We would like to express our sincere gratitude to A. Z. Zinchenko (University of Colorado Boulder) for sharing with us the FORTRAN implementation for computing aerodynamic interactions between liquid particles and many useful suggestions and remarks. We are also genuinely thankful for the valuable comments we have received from D. L. Koch and A. Roy (Cornell University). With their help, we were able to solve several problems encountered during the implementation of the algorithm for computing noncontinuum lubrication forces. This work was supported by National Science Centre, Poland, under Grant No. 2018/30/Q/ST8/00341. We also wish to thank the Interdisciplinary Centre for Mathematical and Computational Modelling (ICM) at the University of Warsaw, for providing computational resources (Grants No. GA73-14 and G87-1145).

APPENDIX A: EXACT SOLUTIONS IN BISPHERICAL COORDINATES

The bispherical coordinate system has been used to solve various physical problems such as interaction of a sphere with infinite rigid or free flat surfaces [45], interaction between two internal eccentric spheres as in a spherical journal bearing [46], or elastic media having two spherical cavities [47]. Here we review relevant studies on analytical solutions for two spherical particles, both rigid and liquid, interacting through an unbounded, quiescent, viscous fluid.

The interaction of two spheres rotating around their line of centers has been investigated by Jeffery [46]. Stimson and Jeffery [35] considered a system with the pair of particles translating in the same direction along their line of centers, i.e., following each other. In turn, Maude [17] developed a solution of the Stokes equation, for two rigid spheres either approaching or retreating along the line of centers. Brenner [45] derived the same force representation for a sphere approaching a *free* plane surface. He also showed that omission of inertial terms from N-S equations, i.e., Stokes regime, counterintuitively leads to having the same magnitude in force whether the sphere moves towards or away from the plane.

Goldman *et al.* [39] solved the symmetrical (flow around two equal-sized spheres) coupled problem of a pair of particles moving in the same direction and rotating with opposite angular velocities around central axes perpendicular to their line of centers. O'Neill [40] found solutions to two problems with boundary conditions complementary to that of Goldman *et al.* [39], namely, a pair of spheres translating in opposite directions and rotating with the same angular velocities about axes perpendicular to the line connecting their centers. These solutions require solving a system of equations for a series of decaying recurrent coefficients. O'Neill and Majumdar [36] generalized this solution to the case of the asymmetric configuration with unequal-sized particles. These studies provide an exact representation of interaction between two *rigid* spheres in a viscous fluid.

By solving the Stokes flow inside the spherical particles, Wacholder and Weihs [38] developed exact solutions for two identical liquid spheres following each other. They also showed that their solution in the limit of very large viscosity ratios approaches the solution by Stimson and Jeffery [35]. This is the case of an extremely viscous internal circulation compared to the external flow. Haber *et al.* [26] generalized the solution to two fluid drops with different sizes and viscosities moving with any orientation along their line of centers. Zinchenko [27] derived the solution for two fluid drops translating normal to that line. These studies provide a complete description of the drag forces acting on a pair of *fluid* spheres.

It has to be added that the studies mentioned above were carried out under the continuum assumption of the fluid, that is, in the limit of zero Knudsen number. In the range of small Knudsen numbers, Reed and Morrison [37] developed a solution for two rigid spheres translating along their line of centers by considering free slip boundary conditions on their surfaces. Their solution approaches those of Wacholder and Weihs [38] or Haber *et al.* [26] in the limit of low viscosity ratio. Grashchenkov [48] and recently Rother *et al.* [6] developed solutions for a pair of fluid drops having free-slip boundary conditions and moving along their line of centers. Their solutions in the limit approach those derived by Reed and Morrison [37] as well as Haber *et al.* [26]. These continuum-slip force representations are valid only for small Knudsen numbers, $Kn < 0.1$.

APPENDIX B: LIST OF MISPRINTS

Rigorous numerical tests were conducted to compare the force and torque representation from the twin multipole expansion method by Jeffrey and Onishi [34] with the solutions developed in bispherical coordinates. The comparison showed us some of the potential misprints in all these studies, some of which were already reported by others. Table I lists these misprints.

APPENDIX C: TABLES OF COLLISION EFFICIENCY

In this Appendix Tables II, III, and IV provide the results of simulations performed in this study. The same values are plotted in Fig. 7.

-
- [1] W. W. Grabowski and L.-P. Wang, Growth of cloud droplets in a turbulent environment, *Annu. Rev. Fluid Mech.* **45**, 293 (2013).
 - [2] L. Brandt and F. Coletti, Particle-laden turbulence: Progress and perspectives, *Annu. Rev. Fluid Mech.* **54**, 159 (2022).
 - [3] K. V. Beard and H. T. Ochs III, Warm-rain initiation: An overview of microphysical mechanisms, *J. Appl. Meteor.* **32**, 608 (1993).
 - [4] M. Voßkuhle, A. Pumir, E. Lévêque, and M. Wilkinson, Prevalence of the sling effect for enhancing collision rates in turbulent suspensions, *J. Fluid Mech.* **749**, 841 (2014).
 - [5] X.-Y. Li, A. Brandenburg, G. Svensson, N. E. Haugen, B. Mehlig, and I. Rogachevskii, Effect of turbulence on collisional growth of cloud droplets, *J. Atmos. Sci.* **75**, 3469 (2018).
 - [6] M. A. Rother, J. K. Stark, and R. Davis, Gravitational collision efficiencies of small viscous drops at finite Stokes numbers and low Reynolds numbers, *Int. J. Multiphase Flow* **146**, 103876 (2022).
 - [7] A. M. Blyth, Entrainment in cumulus clouds, *J. Appl. Meteor.* **32**, 626 (1993).
 - [8] Y. Yin, Z. Levin, T. G. Reisin, and S. Tzivion, The effects of giant cloud condensation nuclei on the development of precipitation in convective clouds—A numerical study, *Atmos. Res.* **53**, 91 (2000).
 - [9] R. A. Shaw, W. C. Reade, L. R. Collins, and J. Verlinde, Preferential concentration of cloud droplets by turbulence: Effects on the early evolution of cumulus cloud droplet spectra, *J. Atmos. Sci.* **55**, 1965 (1998).
 - [10] W. C. Reade and L. R. Collins, A numerical study of the particle size distribution of an aerosol undergoing turbulent coagulation, *J. Fluid Mech.* **415**, 45 (2000).
 - [11] S. Sundaram and L. R. Collins, Collision statistics in an isotropic particle-laden turbulent suspension. Part 1. Direct numerical simulations, *J. Fluid Mech.* **335**, 75 (1997).
 - [12] L.-P. Wang, O. Ayala, B. Rosa, and W. W. Grabowski, Turbulent collision efficiency of heavy particles relevant to cloud droplets, *New J. Phys.* **10**, 075013 (2008).
 - [13] R. H. Davis, The rate of coagulation of a dilute polydisperse system of sedimenting spheres, *J. Fluid Mech.* **145**, 179 (1984).
 - [14] R. H. Pruppacher and J. D. Klett, *Microphysics of Clouds and Precipitation*, Atmospheric and Oceanographic Sciences Library, Vol. 18 (Kluwer Academic Publishers, Dordrecht, The Netherlands, 1997).

- [15] L.-P. Wang, O. Ayala, and W. W. Grabowski, Improved formulations of the superposition method, *J. Atmos. Sci.* **62**, 1255 (2005).
- [16] O. Ayala, W. W. Grabowski, and L.-P. Wang, A hybrid approach for simulating turbulent collisions of hydrodynamically-interacting particles, *J. Comput. Phys.* **225**, 51 (2007).
- [17] A. D. Maude, End effects in a falling-sphere viscometer, *Br. J. Appl. Phys.* **12**, 293 (1961).
- [18] R. H. Davis, J. A. Schonberg, and J. M. Rallison, The lubrication force between two viscous drops, *Phys. Fluids* **1**, 77 (1989).
- [19] R. R. Sundararajakumar and D. L. Koch, Non-continuum lubrication flows between particles colliding in a gas, *J. Fluid Mech.* **313**, 283 (1996).
- [20] L. M. Hocking and P. R. Jonas, The collision efficiency of small drops, *Q. J. Royal Met. Soc.* **96**, 722 (1970).
- [21] B. Rosa, L.-P. Wang, M. R. Maxey, and W. W. Grabowski, An accurate and efficient method for treating aerodynamic interactions of cloud droplets, *J. Comput. Phys.* **230**, 8109 (2011).
- [22] J. Chun and D. L. Koch, Coagulation of monodisperse aerosol particles by isotropic turbulence, *Phys. Fluids* **17**, 027102 (2005).
- [23] J. Dhanasekaran, A. Roy, and D. L. Koch, Collision rate of bidisperse spheres settling in a compressional non-continuum gas flow, *J. Fluid Mech.* **910**, A10 (2021).
- [24] J. Dhanasekaran, A. Roy, and D. L. Koch, Collision rate of bidisperse, hydrodynamically interacting spheres settling in a turbulent flow, *J. Fluid Mech.* **912**, A5 (2021).
- [25] A. Z. Zinchenko, Calculation of hydrodynamic interaction between drops at low Reynolds numbers, *J. Appl. Math. Mech.* **42**, 1046 (1978).
- [26] S. Haber, G. Hetsroni, and A. Solan, On the low Reynolds number motion of two droplets, *Int. J. Multiphase Flow* **1**, 57 (1973).
- [27] A. Z. Zinchenko, The slow asymmetric motion of two drops in a viscous medium, *J. Appl. Math. Mech.* **44**, 30 (1980).
- [28] A. Z. Zinchenko, Calculation of the effectiveness of gravitational coagulation of drops with allowance for internal circulation, *J. Appl. Math. Mech.* **46**, 58 (1982).
- [29] M. K. Yau and R. R. Rogers, *A Short Course in Cloud Physics* (Elsevier, 1996).
- [30] C. K. Batchelor and G. K. Batchelor, *An Introduction to Fluid Dynamics* (Cambridge University Press, 2000).
- [31] S. Kim and S. J. Karrila, *Microhydrodynamics: Principles and Selected Applications* (Courier Corporation, 2013).
- [32] J. S. Hadamard, Mouvement permanent lent d'une sphère liquide et visqueuse dans un liquide visqueux, *C. R. Acad. Sci. (Paris)* **152**, 1735 (1911).
- [33] W. Rybczyński, Über die fortschreitende Bewegung einer flüssigen Kugel in einem zähen Medium, *Bull. Acad. Sci. Cracovie A*, 40 (1911).
- [34] D. J. Jeffrey and Y. Onishi, Calculation of the resistance and mobility functions for two unequal rigid spheres in low-Reynolds-number flow, *J. Fluid Mech.* **139**, 261 (1984).
- [35] M. Stimson and G. B. Jeffery, The motion of two spheres in a viscous fluid, *Proc. R. Soc. Lond.* **111**, 110 (1926).
- [36] M. E. O'Neill and S. R. Majumdar, Asymmetrical slow viscous fluid motions caused by the translation or rotation of two spheres. Part I: The determination of exact solutions for any values of the ratio of radii and separation parameters, *Z. Angew. Math. Phys.* **21**, 164 (1970).
- [37] L. D. Reed and F. A. Morrison, Particle interactions in viscous flow at small values of Knudsen number, *J. Aerosol Sci.* **5**, 175 (1974).
- [38] E. Wacholder and D. Weihs, Slow motion of a fluid sphere in the vicinity of another sphere or a plane boundary, *Chem. Eng. Sci.* **27**, 1817 (1972).
- [39] A. J. Goldman, R. G. Cox, and H. Brenner, The slow motion of two identical arbitrarily oriented spheres through a viscous fluid, *Chem. Eng. Sci.* **21**, 1151 (1966).
- [40] M. E. O'Neill, Exact solutions of the equations of slow viscous flow generated by the asymmetrical motion of two equal spheres, *Appl. Sci. Res.* **21**, 452 (1969).
- [41] S. G. Jennings, The mean free path in air, *J. Aerosol Sci.* **19**, 159 (1988).

- [42] M. H. Davis, Collisions of small cloud droplets: Gas kinetic effects, *J. Atmos. Sci.* **29**, 911 (1972).
- [43] <https://github.com/aababaei/Two-Sphere-Interaction>.
- [44] <https://www.uwo.ca/apmaths/faculty/jeffrey/research/Resistance.html>.
- [45] H. Brenner, The slow motion of a sphere through a viscous fluid towards a plane surface, *Chem. Eng. Sci.* **16**, 242 (1961).
- [46] G. B. Jeffery, On the steady rotation of a solid of revolution in a viscous fluid, *Proc. London Math. Soc.* **S214**, 327 (1915).
- [47] E. Sternberg and M. A. Sadowsky, On the axisymmetric problem of the theory of elasticity for an infinite region containing two spherical cavities, *J. Appl. Mech.* **19**, 19 (1952).
- [48] S. I. Grashchenkov, The effect of slip on the motion of two droplets and of a droplet close to a plane surface of a liquid, *Aerosol Sci. Technol.* **25**, 101 (1996).
- [49] J. Happel and H. Brenner, *Low Reynolds Number Hydrodynamics with Special Applications to Particulate Media* (Martinus Nijhof, 1983).
- [50] B. D. Goddard, R. D. Mills-Williams, and J. Sun, The singular hydrodynamic interactions between two spheres in Stokes flow, *Phys. Fluids* **32**, 062001 (2020).
- [51] V. N. Beshkov, B. P. Radoev, and I. B. Ivanov, Slow motion of two droplets and a droplet towards a fluid or solid interface, *Int. J. Multiphase Flow* **4**, 563 (1978).
- [52] A. K. Townsend, The mechanics of suspensions, Ph. D. thesis, University College London, 2017.
- [53] K. Ichiki, Errata on the papers for two-body exact solutions in Stokes flows, <http://ryuon.sourceforge.net/twobody/errata.html>.
- [54] A. J. C. Ladd, Hydrodynamic transport coefficients of random dispersions of hard spheres, *J. Chem. Phys.* **93**, 3484 (1990).
- [55] M. A. Rother, Effects of incompressible surfactant on thermocapillary interactions of spherical drops, *Int. J. Multiphase Flow* **35**, 417 (2009).